NATIONAL ADVISORY COMMITTEE FOR AERONAUTICS

TECHNICAL NOTE

No. 1337

EFFECT OF HORIZONTAL-TAIL POSITION ON THE HINGE MOMENTS OF AN UNBALANCED RUDDER IN ATTITUDES SIMULATING SPIN CONDITIONS

By Ralph W. Stone, Jr. and Sanger M. Burk, Jr.

Langley Memorial Aeronautical Laboratory
Langley Field, Va.

Washington
June 1947

NATIONAL ADVISORY COMMITTEE FOR AERONAUTICS

TECHNICAL NOTE NO. 1337

EFFECT OF HORIZONTAL-TAIL POSITION ON THE HINGE MOMENTS OF AN UNBALANCED RUDDER IN ATTITUDES SIMULATING SPIN CONDITIONS

By Ralph W. Stone, Jr. and Sanger M. Burk, Jr.

SUMMARY

An investigation was made in the Langley 15-foot free-spinning tunnel to determine the effect of horizontal-tail position on rudder hinge moments in attitudes simulating spinning conditions. Hinge-moment measurements were made on an unbalanced rudder on a rectangular vertical tail for six positions of the horizontal tail. The hinge-moment measurements were supplemented by tuft tests to determine the air flow about the vertical tail.

The results of this investigation are based on the rudder-pedal forces of the airplane without regard to the effectiveness of the rudder in producing recovery from a spin. In general, the results indicated that a low rearward position of the horizontal tail gave the smallest rudder hinge-moment coefficients, which, in turn, indicated that the rudder shielding was greater for this position of the horizontal tail than for other positions. Conversely, a high forward position gave the largest rudder hinge-moment coefficients, which indicated the least rudder shielding for this horizontal-tail position. The results of tuft observations of air flow about the vertical tail substantiated these results. The rudder hinge-moment coefficients generally decreased in magnitude with increased angle of attack for all horizontal-tail positions. The effect of rudder deflection on rudder hinge-moment coefficient was not appreciably affected by the horizontal-tail positions except in very flat spins. Computations of rudder-pedal forces based on the results of the tests and upon empirical drag-coefficient data of spinning models indicate that for all tail positions the highest forces are obtained at the lowest angle of attack in the spin. The pedal forces for airplanes in the light-airplane category are well within the capabilities of the pilot for all angles of attack. For heavier airplanes, the rudder may require some form of balance, particularly if the spins are steep.

INTRODUCTION

The problem of spin recovery is considered to be one of great importance for all airplane designs. Methods of obtaining effective tail designs for spin recovery of airplanes have been presented in reference 1. Such tail designs, however effective, do not produce recovery if the controls cannot be moved as such movement is generally necessary for recovery. The control forces of either the elevator or the rudder may be excessive and thus recovery may be prevented. Estimations of elevator hinge moments and the corresponding stick forces in spins have been presented in reference 2. The present investigation was undertaken to provide general information on the pedal forces in spins without regard to the effectiveness of the rudder in producing recovery.

At the high angles of attack encountered with a spinning airplane the vertical tail may be shielded by the horizontal tail, fuselage, or wing. The present investigation provides information on pedal forces in spins with particular reference to the effect of the position of the horizontal tail. The wake of the horizontal tail may shield the vertical tail and influence the rudder control force — the extent, in general, depending on the relative positions of the horizontal and vertical tails.

The tests were performed in the Langley 15-foot free-spinning tunnel with an unbalanced rudder and elevator on rectangular vertical and horizontal tails. The hinge-moment measurements were supplemented by tuft tests to determine the general nature of the air flow about the vertical tail at high angles of attack. Six different positions of the horizontal tail were investigated as well as the vertical tail alone.

COEFFICIENTS AND SYMBOLS

C_h rudder hinge-moment coefficient $\left(H/qb_r\bar{c}_r^2\right)$

C_D drag coefficient of airplane (D/qS)

F rudder-pedal force (positive when push force is on right rudder pedal), pounds

H rudder hinge moment (positive when it tends to deflect rudder to left), foot-pounds

q dynamic pressure, pounds per square foot $\left(\frac{\rho V^2}{2}\right)$

ρ mass density of air, slugs per cubic foot

V true rate of descent, feet per second

b_r rudder height, feet

$\bar{c}_r$ root-mean-square chord of rudder (rearward of hinge axis), feet

D drag of airplane, pounds

S wing area, square feet

W normal gross weight of airplane, pounds

l_r total rudder-pedal travel (assumed as 0.54 ft), feet

δ_r rudder deflection with respect to fin (positive when trailing edge is to left), degrees

α angle of attack referred to chord of horizontal tail, degrees

ψ angle of yaw (positive when nose of airplane is to right of flight path), degrees

β angle of sideslip (positive when relative wind comes from right of plane of symmetry), degrees

$C_{h_{\delta_r}}$ rate of change of rudder hinge-moment coefficient with rudder deflection

C_{h_ψ} rate of change of rudder hinge-moment coefficient with angle of yaw

APPARATUS

A plan view and side view of the rectangular vertical and horizontal tails used for the tests are presented in figure 1. A sketch of the model mounted in the Langley 15-foot free-spinning tunnel with a dashed outline of a fuselage sketched in for reference is shown in figure 2. Figure 3 is a photograph of the vertical tail alone mounted in the tunnel. A photograph of the tail assembly with the horizontal tail in a typical position (low center position) in the tunnel is presented in figure 4. The tails were made of laminated mahogany and had NACA 0009 airfoil sections; and the elevator and rudder chords were 33.3 percent of the airfoil chord. The gaps between the movable and fixed surfaces were unsealed. The elevator and rudder had no aerodynamic balance. The rudder, however, was mass

balanced so that no moment would be exerted on the strain gage because of the weight of the rudder.

The six combinations of the horizontal tail mounted on the vertical tail are sketched in figure 5 and are as follows:

Position I: The low forward position for which the chord line of the horizontal tail was 1 inch above the bottom of the vertical tail and the elevator hinge line was forward of the rudder hinge line by approximately $\frac{1}{4}$ rudder chord.

Position II: The low center position for which the chord line of the horizontal tail was 1 inch above the bottom of the vertical tail and the elevator hinge line coincided with the rudder hinge line.

Position III: The low rearward position for which the chord line of the horizontal tail was 1 inch above the bottom of the vertical tail and elevator hinge line was rearward of the rudder hinge line by 1 rudder chord.

Position IV: The high forward position for which the chord line of the horizontal tail was at a height midway of the vertical tail and the elevator hinge line was forward of the rudder hinge line by approximately 1 rudder chord.

Position V: The high center position for which the chord line of the horizontal tail was at a height midway of the vertical tail and the elevator hinge line coincided with the rudder hinge line.

Position VI: The high rearward position for which the chord line of the horizontal tail was at a height midway of the vertical tail and the elevator hinge line was rearward of the rudder hinge line by 1 rudder chord.

The dimensional characteristics of the horizontal and vertical tails are as follows:

Vertical tail surfaces:	
Total area, square inches	216
Span, inches	18
Chord, inches	12
Rudder root-mean-square chord, inches	4
Aspect ratio	1.5
Rudder area for positions I, II, IV, and V, square inches	72
Rudder area for position III, square inches	65.25
Rudder area for position VI, square inches	67.00
Airfoil section	NACA 0009

Horizontal tail surfaces:	
Total area, square inches	414.26
Span, inches	36
Chord, inches	12
Aspect ratio	3.13
Elevator area, square inches	126.26
Airfoil section	NACA 0009

Because of construction difficulties, the horizontal tail was actually moved 4.38 inches forward of the rudder hinge line for the forward position, whereas in the rearward position it was 4.00 inches (1 rudder chord) rearward of the rudder hinge line. For the two rearward positions of the horizontal tail (positions III and VI) cut-outs were necessary in the lower and center parts (respectively) of the rudder to allow it to swing over the stabilizer. (See fig. 1.) A second rudder was constructed with cut-outs for these rearward horizontal-tail positions. A cut-out, made in the elevator (fig. 1) to allow the rudder to swing through its desired range for horizontal-tail positions II and V, was retained for all other tail positions.

The elevator and rudder were held by a friction clamp at the desired deflection on the hinge rod, and all deflections were set by templets. The rudder hinge moments were measured electrically by a strain gage. This gage was calibrated by applying a series of known moments to the rudder.

The tufts used to determine the general nature of the air flow about the vertical tail were fine silk threads approximately $1\frac{1}{4}$ inches in length. Two rows of tufts at approximately 1-inch intervals were attached to each side of the vertical tail by Scotch cellulose tape; one row was placed along the fin and the other was placed along the rudder.

TESTS

The tests were conducted in the Langley 15-foot free-spinning tunnel which has a turbulence factor of 1.78. All tests were made at a dynamic pressure of 2.66 pounds per square foot, which corresponds to an airspeed of 32.3 miles per hour under standard sea level conditions.

The attitude of the tail assembly was varied to give the desired angles of attack and sideslip. The angle of sideslip was simulated by the angle of yaw as shown in figure 2. The desired values of sideslip were obtained by yawing the model about the stability Z-axis, which is perpendicular to the vertically rising airstream. The stability axes are defined as an orthogonal system of axis in which the Z-axis is in the plane of symmetry and perpendicular to the relative wind, the X-axis

is in the plane of symmetry and perpendicular to the Z-axis, and the Y-axis is perpendicular to the plane of symmetry.

Hinge-Moment Tests

In order to simulate spinning conditions for the hinge-moment tests, the model was tested throughout an angle-of-attack range from 0° to 90° in 10° increments and through a yaw range of 30° to −30° in 10° increments. The angles of yaw as set on the model may be interpreted as angles of sideslip that would be encountered at the tail of an airplane in a spin. The actual angle of sideslip is equal in magnitude to the angle of yaw but has the opposite sign. The angles of attack as set represent the angles of attack of the stabilizer and not angles of attack of the vertical tail as an airfoil. The rudder at each angle of attack and yaw angle was deflected from 0° to 30° in 10° increments. For the foregoing conditions, the vertical tail was tested with the horizontal tail in each of the six positions and also with the horizontal tail removed. The elevator deflection was zero for all tests.

As there was no fin offset, results obtained with a positive rudder deflection may also be considered as representative of negative rudder deflection provided the hinge-moment coefficient signs are reversed. Each configuration, therefore, represents a spin with the rudder set either with or against the spin. For example, a negative angle of yaw with left rudder may be considered as representative of outward sideslip in a left spin with rudder with the spin or of inward sideslip in a right spin with rudder against the spin. Similarly, a positive angle of yaw with left rudder may be considered as representative of outward sideslip in a right spin with rudder against the spin or of inward sideslip in a left spin with rudder with the spin. Table I shows in detail how the various figures may be interpreted for a right or left spin and how the angles of yaw may be interpreted to represent sideslip.

Tuft Tests

Tuft tests were made on the vertical tail for various positions of the horizontal tail and for the condition with the horizontal tail removed. These tests were arbitrarily made at angles of attack of 0°, 10°, 20°, 50°, and 80° and for angles of yaw of 0° and −15° when the horizontal tail was installed and for 0° and ±20° when the horizontal tail was removed.

CORRECTIONS

No corrections were made for the effect of the tunnel walls on the tail surfaces as the size of the surfaces was small compared to the

diameter of the tunnel and the corrections would therefore be negligible. Strut interference effects have also been neglected. At first the rectangular wooden arm which supported the vertical tail (fig. 3) was expected to cause an increase in the effective aspect ratio of the vertical tail. The hinge-moment tests with the horizontal tail removed, however, gave coefficients of the order expected for a rudder on a tail of aspect ratio 1.5 as computed exclusive of the supporting member which indicates negligible interference effects.

RESULTS AND DISCUSSION

Rudder Hinge Moments

Rudder hinge-moment coefficients obtained from tests of the vertical tail in various combinations with the horizontal tail are presented in figures 6 to 14. In order to show the shielding effect of the horizontal tail on the vertical tail, the hinge-moment coefficients obtained from tests of the vertical tail alone have been plotted on these same figures. The analysis of these data is based on aerodynamic forces on the rudder without regard to any frictional or centrifugal forces that may exist on the airplane control surfaces in a spin.

Effect of angle of attack on rudder hinge-moment coefficients.- The variation of rudder hinge-moment coefficient with angle of attack for various positions of the horizontal tail and with the horizontal tail removed are presented in figures 6 to 9. The rudder hinge-moment coefficients for all positions of the horizontal tail decreased in magnitude from those for the vertical tail alone; this amount of decrease increased, in general, with angle of attack. The coefficients changed with angle of attack so that they generally approached the line of zero hinge-moment coefficient at very high angles of attack.

In a very few cases the hinge-moment coefficients of the rudder in the presence of the horizontal tail changes sign from those of the rudder alone. This tendency is analogous to overbalancing in that the rudder tends to float in the direction opposite to that expected.

In general, the high forward position of the horizontal tail (position IV) led to the highest values of rudder hinge-moment coefficient, whereas the low rearward position (position III) led to the lowest values. These results indicate that position IV produced the least rudder shielding or blanketing effect, whereas position III produced the most shielding. The shielding effect of the horizontal tail on the vertical tail was small at low angles of attack (0° to 10°) but increased as the angle of attack increased. The relative difference in the shielding effect caused by tail position was small at low angles of attack (0° to 20°) but generally increased as the angle of attack increased up to angles of attack of about 80°, beyond which the relative difference tended to decrease again.

Effect of rudder deflection on rudder hinge-moment coefficients.- The variation of rudder hinge-moment coefficient with rudder defloction for various angles of yaw is presented in figures 10 to 12. These figures are cross plots of figures 6 to 9 for a range of angles of yaw most commonly encountered in spins. The slope $C_{h_{\delta_r}}$ was not greatly affected by the installation of the horizontal tail on the vertical tail or by the various positions of the horizontal tail at low and moderate angles of attack but decreased negatively an appreciable amount at high angles of attack (60° and 80°) which simulate the conditions for very flat spins.

Effect of yaw on rudder hinge-moment coefficients.- The variation of rudder hinge-moment coefficient with angle of yaw for rudder deflections of 0° and 30° is presented in figures 13 and 14. The specific rudder deflections of 0° and 30° were chosen to represent neutral and full rudder deflection in a spin. These figures were obtained by cross-plotting from figures 6 to 9.

The slope C_{h_ψ} was not appreciably affected by the installation of horizontal tail at low angles of attack. In the normal spinning range of angle of attack (30° to 50°) and for high angles of attack, however, there was a marked change in the slopes. As previously indicated, the slope $C_{h_{\delta_r}}$ was not affected in the normal range of angle of attack. Therefore, the direct effect of shielding of the rudder by the horizontal tail in the normal spinning range of angle of attack is to change the values of C_{h_ψ}.

Tuft Tests

Some indication of the shielding effect of the horizontal tail on the vertical tail was obtained from tuft observations. The results of the tuft tests are presented in figures 15 to 21. The photographs give some indication of the shielding effect of the horizontal tail on the vertical tail and in general substantiate the results of the hinge-moment tests.

Application of Hinge-Moment Data

The hinge-moment coefficients presented herein may be used to estimate the rudder-pedal forces required to reverse the rudder on an airplane in a spin, provided that the angle of attack and sideslip at the tail are known. The rudder-pedal force is

$$F = C_h q \bar{c}_r^2 b_r \frac{\delta_r \pi}{180 l_r}$$

In a steady spin the weight of an airplane equals its drag; therefore,

$$W = D = C_D qS$$

or

$$q = \frac{W/S}{C_D}$$

By substitution, then,

$$F = C_h \frac{W/S}{C_D} \bar{c}_r^2 b_r \frac{\delta_r \pi}{180 l_r} \qquad (1)$$

The variation of drag coefficient with angle of attack for a spinning airplane is given in figure 22. This curve was determined from an average of experimental values obtained from spin-tunnel tests of numerous models.

In order to illustrate this method of computing the rudder-pedal forces for a specific design, the following example is given. Consider an airplane that has a tail configuration similar to the high rearward position of the horizontal tail (position VI), a normal gross weight of 8000 pounds, a wing area of 270 square feet $\left(\frac{W}{S} = 29.6 \text{ lb/sq ft}\right)$, and a vertical tail area of 25 square feet. Assume that the airplane is spinning to the right at an altitude of 15,000 feet at an angle of attack of 30° with 20° outward sideslip at the tail and that the rudder is deflected 30° against the spin. From figure 22, the drag coefficient is found to be 0.74. The rudder-pedal force can now be determined. The total pedal travel is assumed to be 0.54 feet and the total rudder deflection, 60°. The rudder dimensions are assumed to be proportional to those of the model used in the current tests (b_r, 6.12 ft and $\bar{c}_r$, 1.36 ft). From table I, if the airplane is assumed to be in a right spin, the rudder 30° against the spin, and the sideslip 20° outward, the figure that applies to this condition can be determined. In this case, the figure is 9(b) and the value of the hinge-moment coefficient is −0.255. Thus, substituting this value in the force formula (equation (1)) gives a rudder-pedal force of −222 pounds. This push force is that which is required on the left pedal to move the rudder fully against the spin.

In order to determine the magnitude of the rudder-pedal forces likely to be encountered with airplanes in a spin, computations have been made for three representative sizes of airplanes for different horizontal-tail positions and for the vertical tail alone. The airplanes represented are light-airplane, fighter, and light-bomber types. Weights of 1500, 10,000, and 20,000 pounds were chosen, respectively, for these types. The wing areas used for the three types were 165, 305, and 475 square feet, respectively, and respective vertical tail areas of 12.0, 28.5, and 55.5 square feet were used. These areas were determined from an average of areas for numerous airplane designs tested in the spin

tunnel. The proportions of the vertical tail and rudder were assumed to be proportional to those of the model used for the current hinge-moment tests. For these computations, the angle of sideslip assumed was zero, the rudder deflection used was 30°, and the value of ρ was arbitrarily taken at an altitude of 15,000 feet. The results of the computations are plotted on figure 23.

For airplanes in the light-airplane category (fig. 23(a)), it appears that, for any position of the horizontal tail or for the vertical tail alone, the rudder-pedal force required to set the rudder against the spin in no case exceeds 140 pounds. This force is much smaller than the maximum of approximately 400 pounds that a pilot can exert on a rudder pedal. (See reference 3.) Figure 23(a) also indicates that the horizontal-tail position affects the rudder-pedal forces of light airplanes only slightly, because the maximum force for any horizontal-tail position or for the vertical tail alone is relatively small. Only one curve was drawn through the numerous points for the various positions of the horizontal tail in this particular figure. Thus, for a light airplane it seems that the rudder-pedal forces encountered in spins should be well within the capabilities of a pilot regardless of horizontal-tail position.

For larger and heavier airplanes (fig. 23(b) and 23(c)) the pedal force is shown to be larger at any given angle of attack because of the larger control surface and because of the increase in rate of descent in the spin.

If a fighter airplane spins at an angle of attack of 30° or greater (fig. 23(b)), or if a light bomber airplane spins at an angle of attack of 50° or greater (fig. 23(c)), the rudder-pedal force necessary to reverse the rudder at these attitudes should be within the pilot's capabilities. Below these respective angles of attack, however, some type of rudder-balance or booster system may be used to overcome the excessive forces. For example, in figure 23(c) a light bomber, spinning at an angle of attack of 30° with the horizontal tail in the low rearward position (position III), must have at least 30 percent of the unbalanced rudder force balanced out in order to bring the pedal forces within the limits of the forces that the pilot can exert.

In general, from an angle of attack of 10° to 40° (fig. 23(b) and 23(c)), the force gradient for all horizontal-tail positions was very steep, which indicates that a small change in angle of attack led to a large change in pedal force. This result may be taken as an indication that, as the angle of attack decreases during the recovery, the pedal force required to maintain the rudder full against the spin increases. The low rearward position (position III) of the horizontal tail, in general, required the smallest pedal force to reverse the rudder fully or to maintain it full against the spin for any given angle of attack,

whereas the high forward position (position IV) required the largest force. Spin-tunnel results have indicated that, for the low rearward positions of the horizontal tail the rudder may be ineffective in producing a recovery and, for high forward positions of the horizontal tail, the rudder is generally effective in producing a recovery. Thus, for high forward positions of the horizontal tail maintaining the rudder full against the spin may not be necessary to obtain a satisfactory recovery, and such horizontal-tail positions may therefore not necessarily require large pedal forces for satisfactory recoveries.

CONCLUSIONS

The results of the investigation to determine the effect of horizontal-tail position on the rudder hinge-moment coefficients and pedal-force characteristics of an unbalanced rudder with rectangular plan form in attitudes simulating spin conditions indicate the following general conclusions without regard to the effectiveness of the rudder in producing a recovery:

1. The low rearward position of the horizontal tail gave the smallest rudder hinge-moment coefficients and pedal forces, which thus indicates that the shielding effect of this position was large relative to the other horizontal-tail positions. Conversely, the high forward position gave the largest hinge-moment coefficients and pedal forces which indicates that the relative shielding effect of this position was small. Tuft observations substantiated these relative shielding effects.

2. The rudder hinge-moment coefficients generally decreased with an increase in angle of attack for all horizontal-tail positions.

3. The rate of change of the rudder hinge-moment coefficient with rudder deflection was not appreciably affected by the horizontal-tail position except in very flat spins.

4. The rudder-pedal force for a light airplane for recovery from a spin should be well within the capabilities of the pilot. For heavier airplanes, the rudder may require some form of balance, particularly if the spins are steep.

5. The pedal force required for full rudder reversal for recovery from a spin increases rapidly as the airplane angle of attack in the spin decreases, especially at relatively low angles of attack.

Langley Memorial Aeronautical Laboratory
National Advisory Committee for Aeronautics
Langley Field, Va., March 26, 1947

REFERENCES

1. Neihouse, Anshal I., Lichtenstein, Jacob H., and Pepoon, Philip W.: Tail-Design Requirements for Satisfactory Spin Recovery. NACA TN No. 1045, 1946.

2. Seidman, Oscar, and Klinar, J. W.: Elevator Stick Forces in Spins as Computed from Wind-Tunnel Measurements. NACA ARR, Oct. 1942.

3. Gough, M. N., and Beard, A. P.: Limitations of the Pilot in Applying Forces to Airplane Controls. NACA TN No. 550, 1936.

TABLE I

INTERPRETATION OF RUDDER HINGE-MOMENT COEFFICIENT CURVES FOR RIGHT OR LEFT SPIN

Rudder deflection, δ_r	Direction of sideslip (right spin)[b]					
With spin[a]	0	Inward	Outward	---	---	---
Neutral	---	---	---	0	Outward	Inward
Against spin	0	Outward	Inward	---	---	---
	Direction of sideslip (left spin)[b]					
With spin	0	Inward	Outward	---	---	---
Neutral	---	---	---	0	Inward	Outward
Against spin[a]	0	Outward	Inward	---	---	---
Read C_h from figs.-	7(d) 8(d) 9(d)	7(a), (b), (c) 8(a), (b), (c) 9(a), (b), (c)	7(e), (f), (g) 8(e), (f), (g) 9(e), (f), (g)	6(d)	6(a), (b), (c),	6(e), (f), (g)

[a]Sign of rudder hinge-moment coefficient, deflection, and angle of yaw must be reversed for this condition.

[b]Sideslip at the tail of the airplane is opposite in sign and equal in magnitude to values of ψ presented in figures.

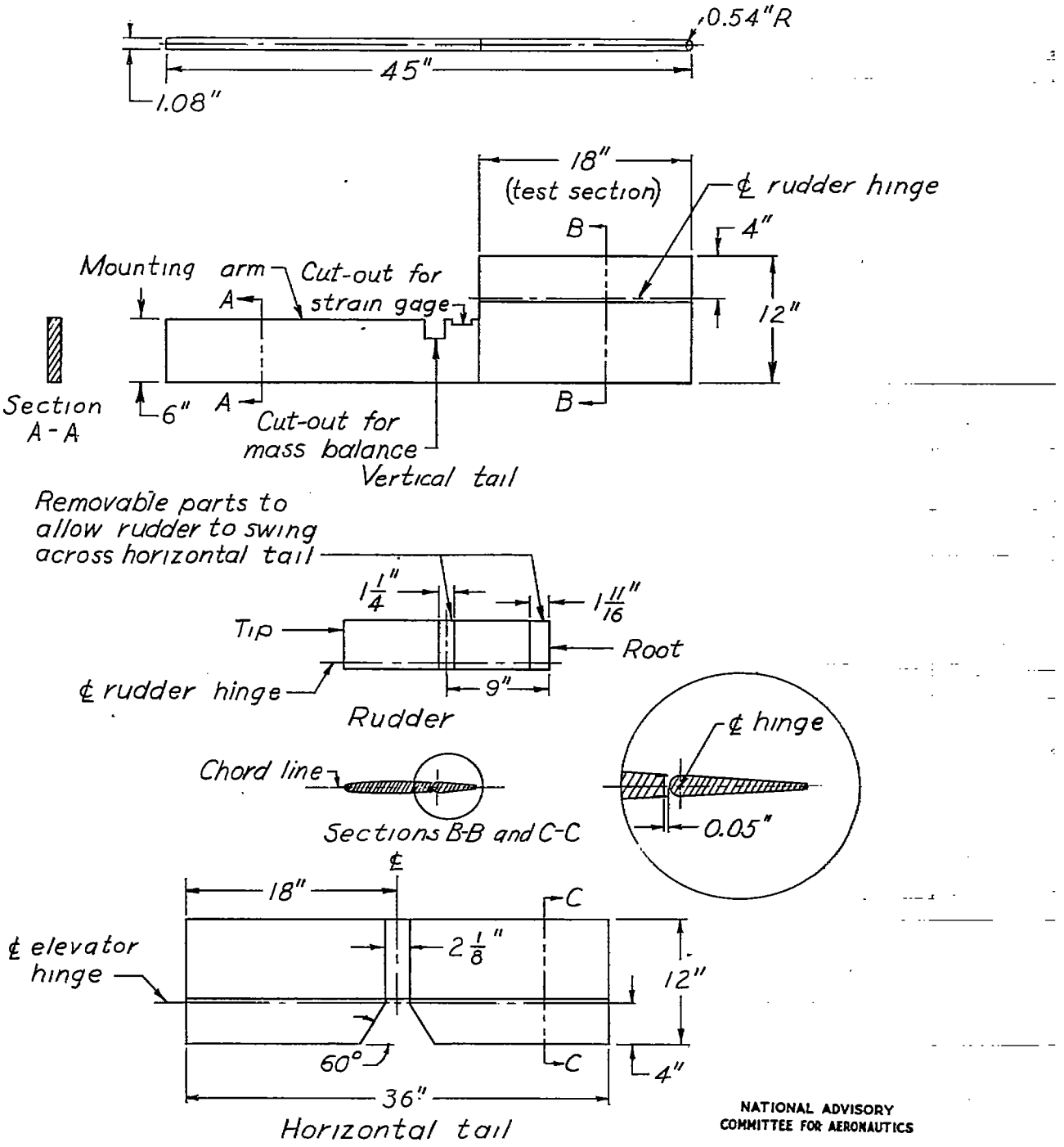

Figure 1.- Plan and side views of the rectangular vertical and horizontal tails. Dimensions are full scale.

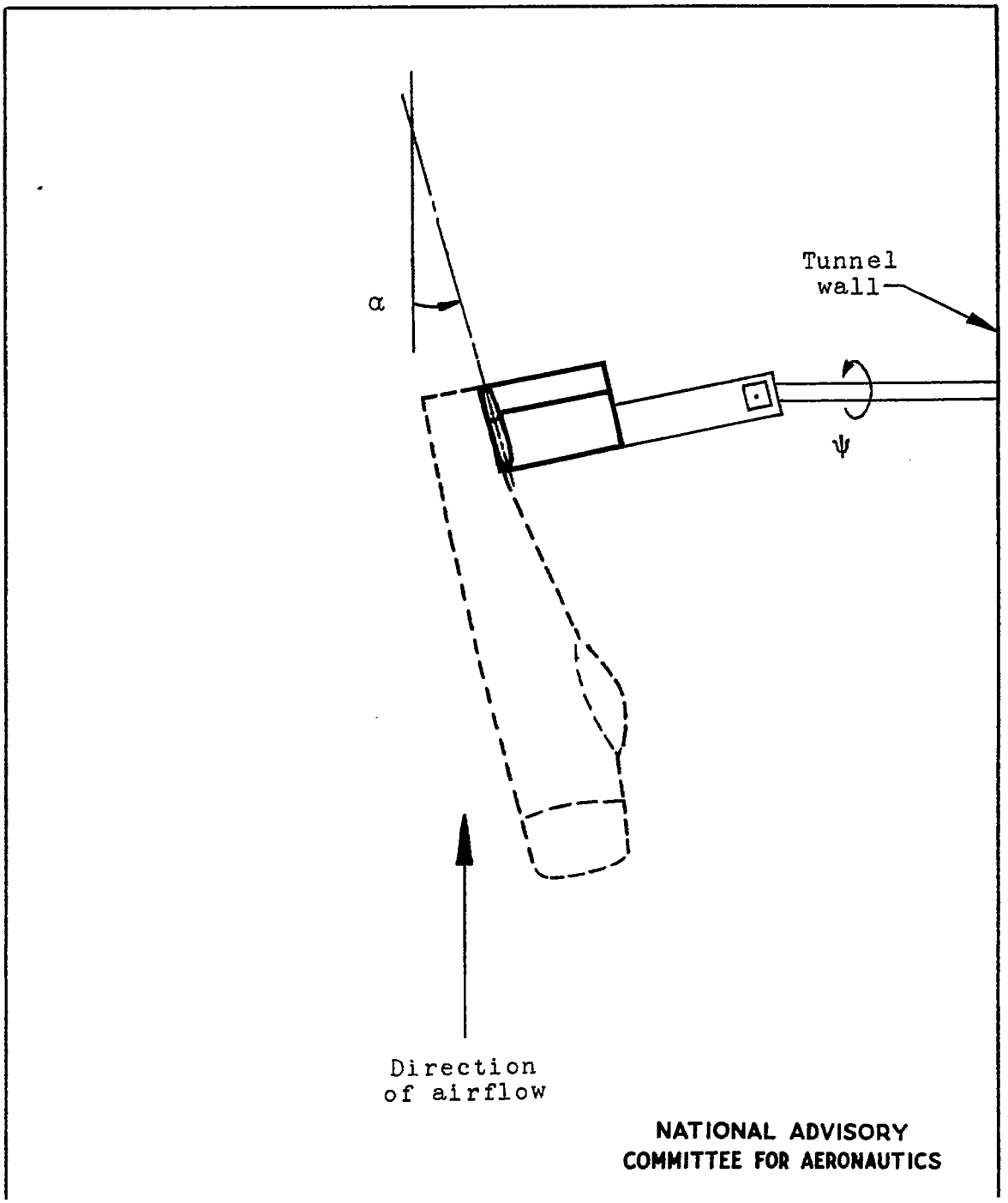

Figure 2.- Horizontal and vertical tail in attitude simulating spin with fuselage of airplane sketched in for reference. Arrows indicate direction of positive values of angles.

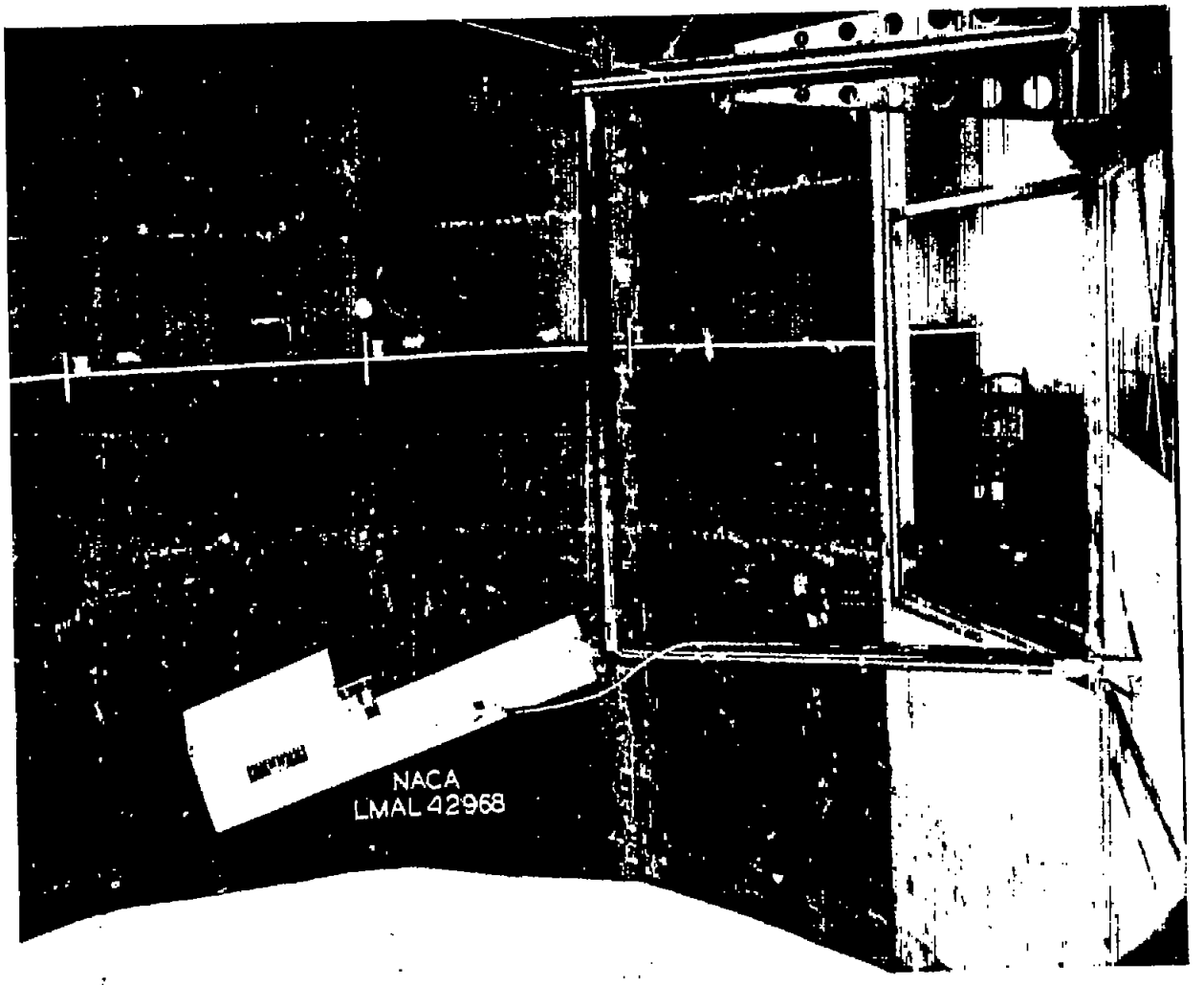

Figure 3.- Vertical tail mounted in Langley 15-foot free-spinning tunnel.

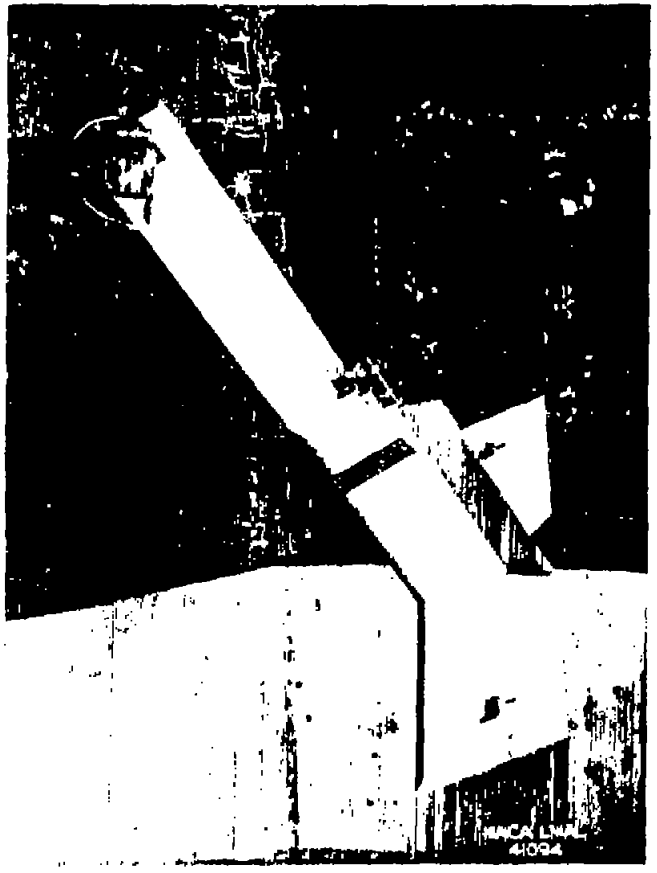

(a) Left-side view.

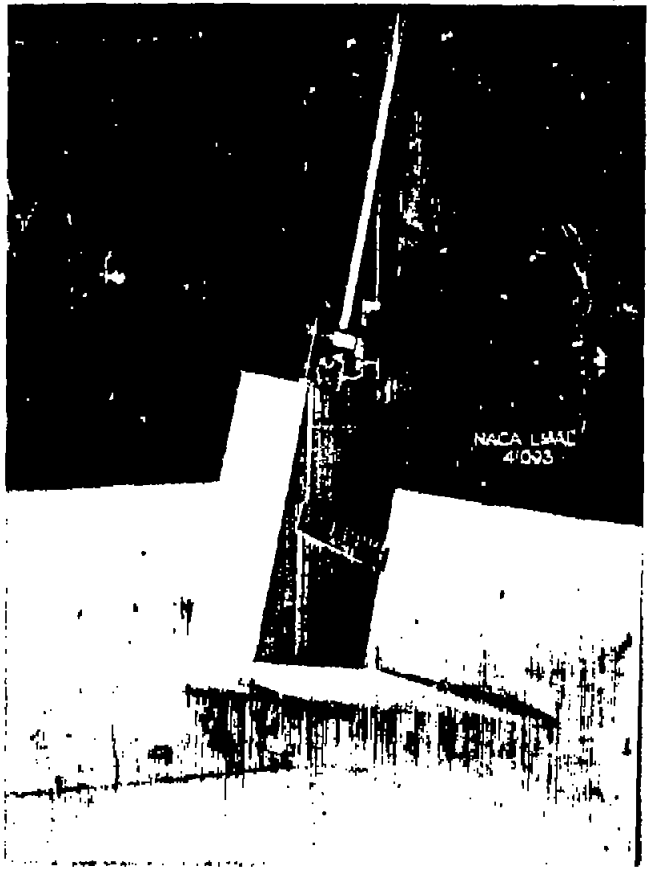

(b) Right-side view.

Figure 4.- Photographs of vertical tail with horizontal tail in position II.

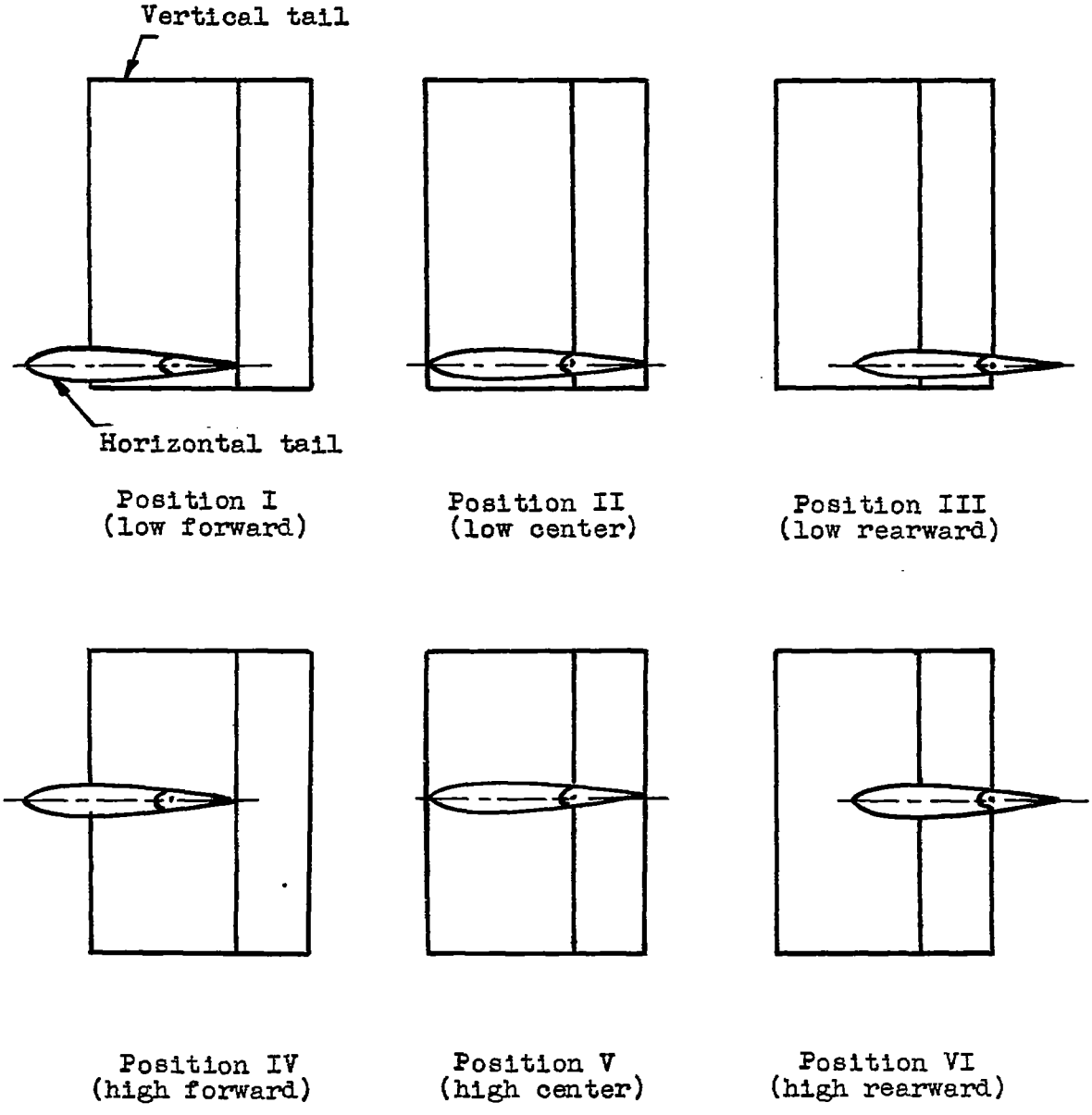

NATIONAL ADVISORY
COMMITTEE FOR AERONAUTICS

Figure 5.- Sketches of vertical tail in six combinations with horizontal tail.

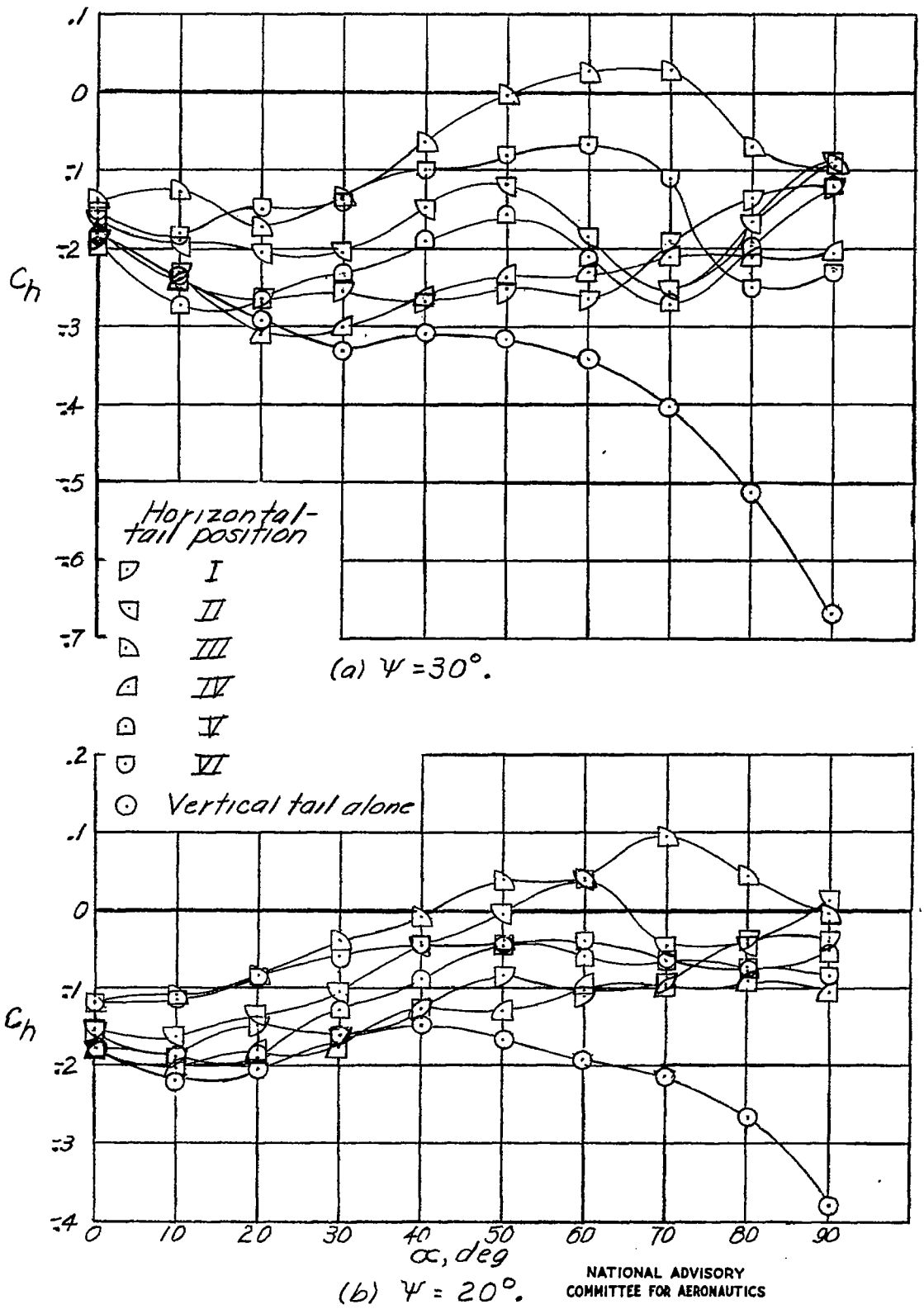

Figure 6.- Rudder hinge-moment coefficient as a function of angle of attack at $\delta_r = 0°$ for various angles of yaw and positions of horizontal tail.

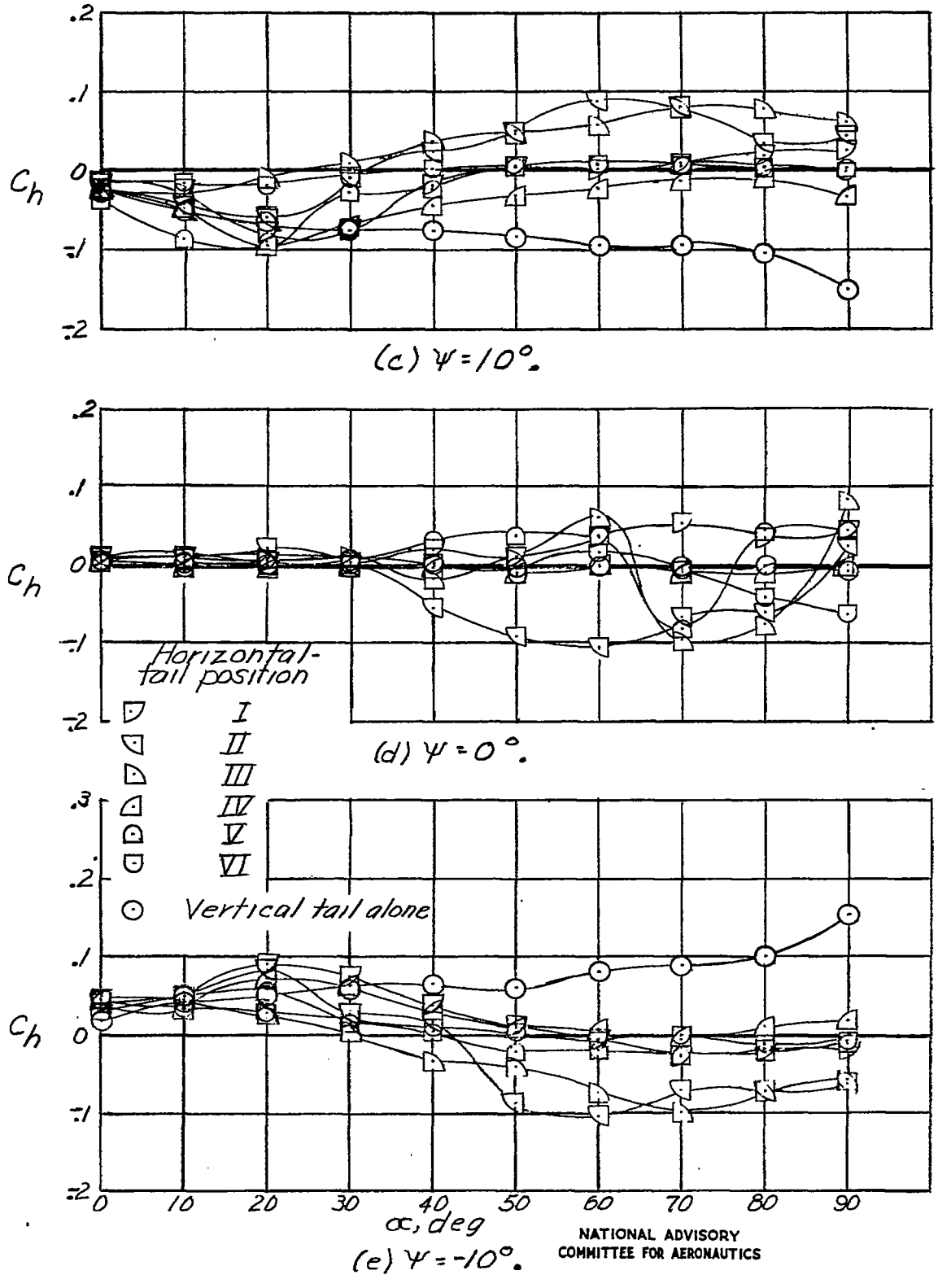

Figure 6.- Continued.

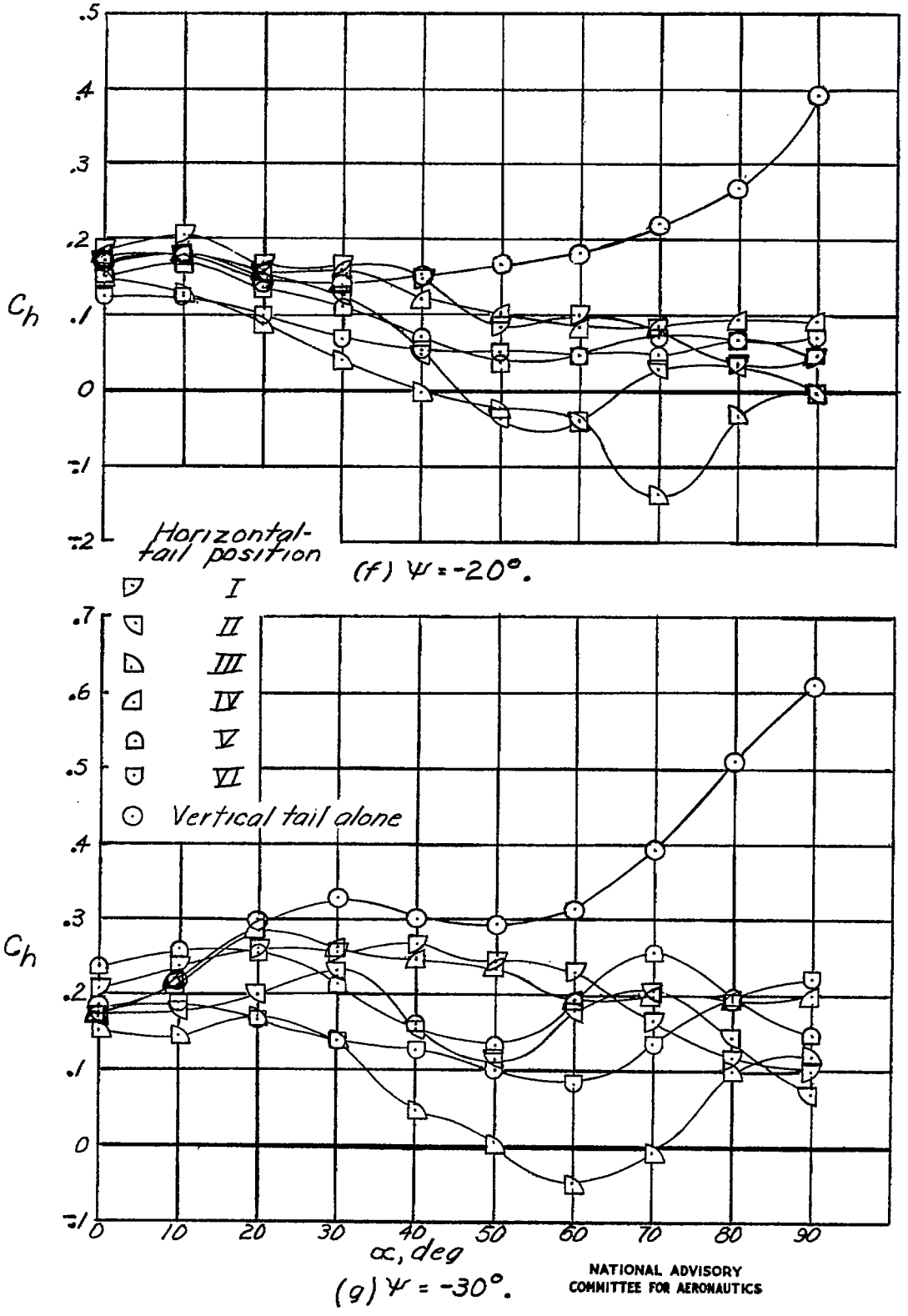

Figure 6.- Concluded.

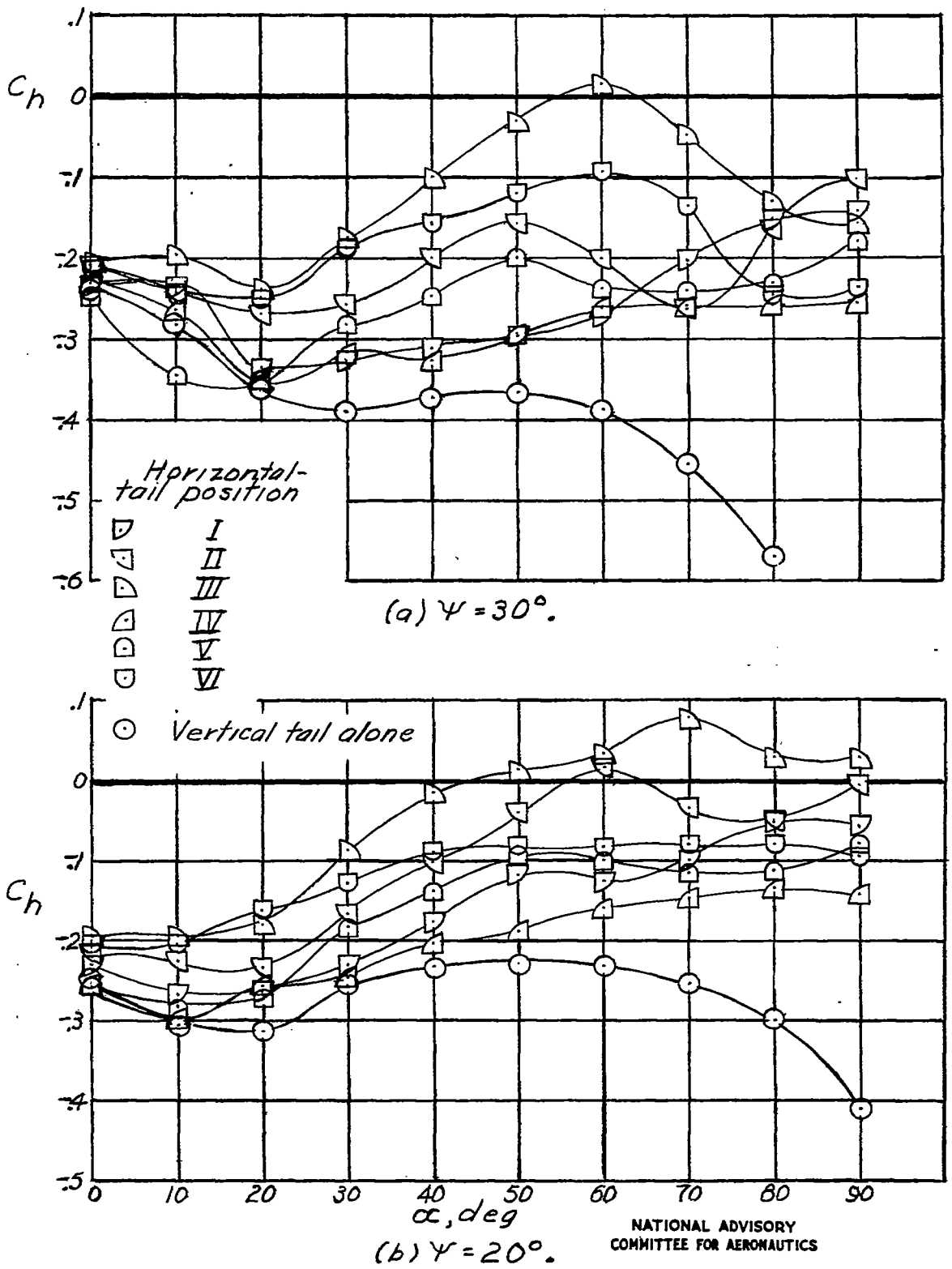

Figure 7.- Rudder hinge-moment coefficient as a function of angle of attack at $\delta_r = 10°$ for various angles of yaw and positions of horizontal tail.

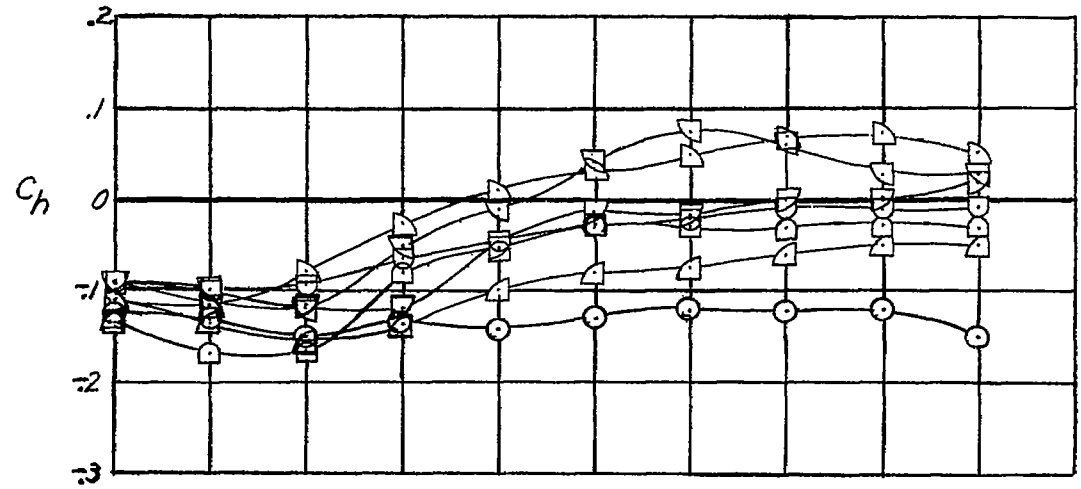

(c) $\Psi = 10°$.

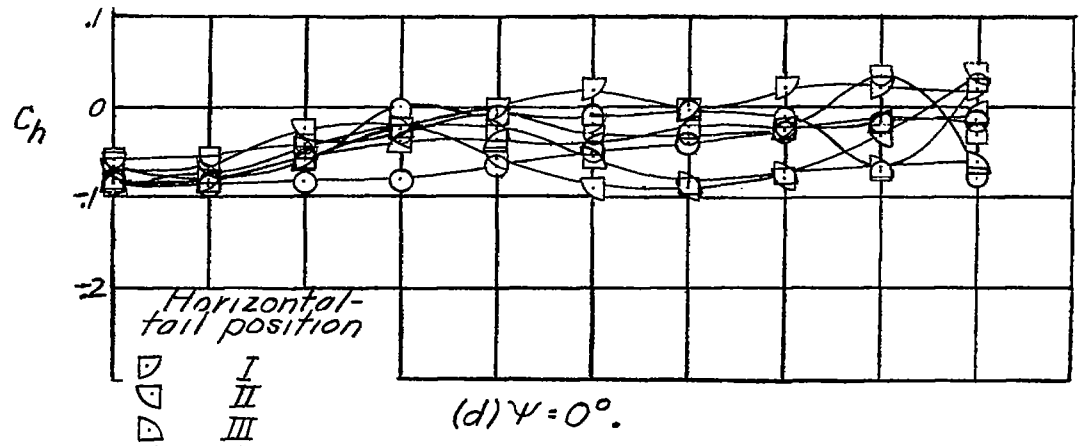

(d) $\Psi = 0°$.

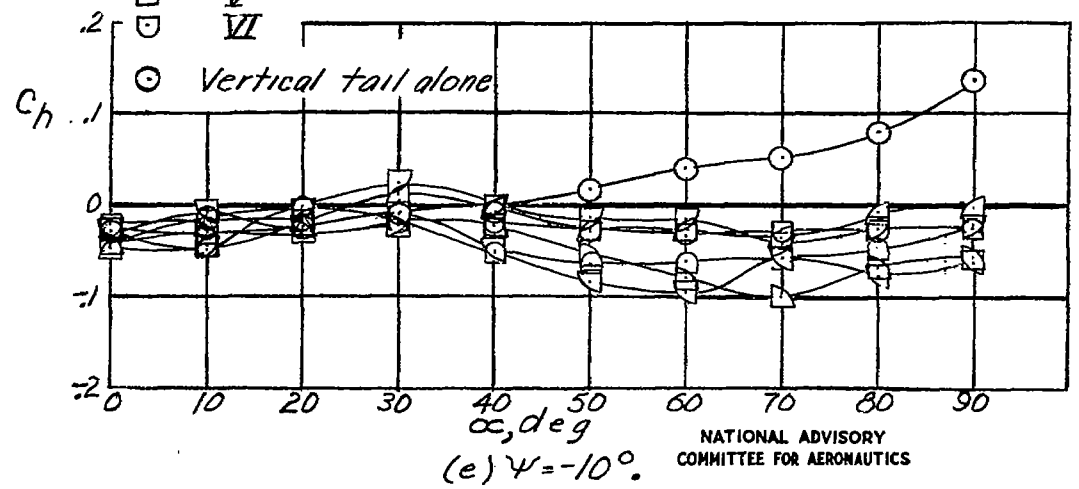

(e) $\Psi = -10°$.

NATIONAL ADVISORY COMMITTEE FOR AERONAUTICS

Figure 7.- Continued.

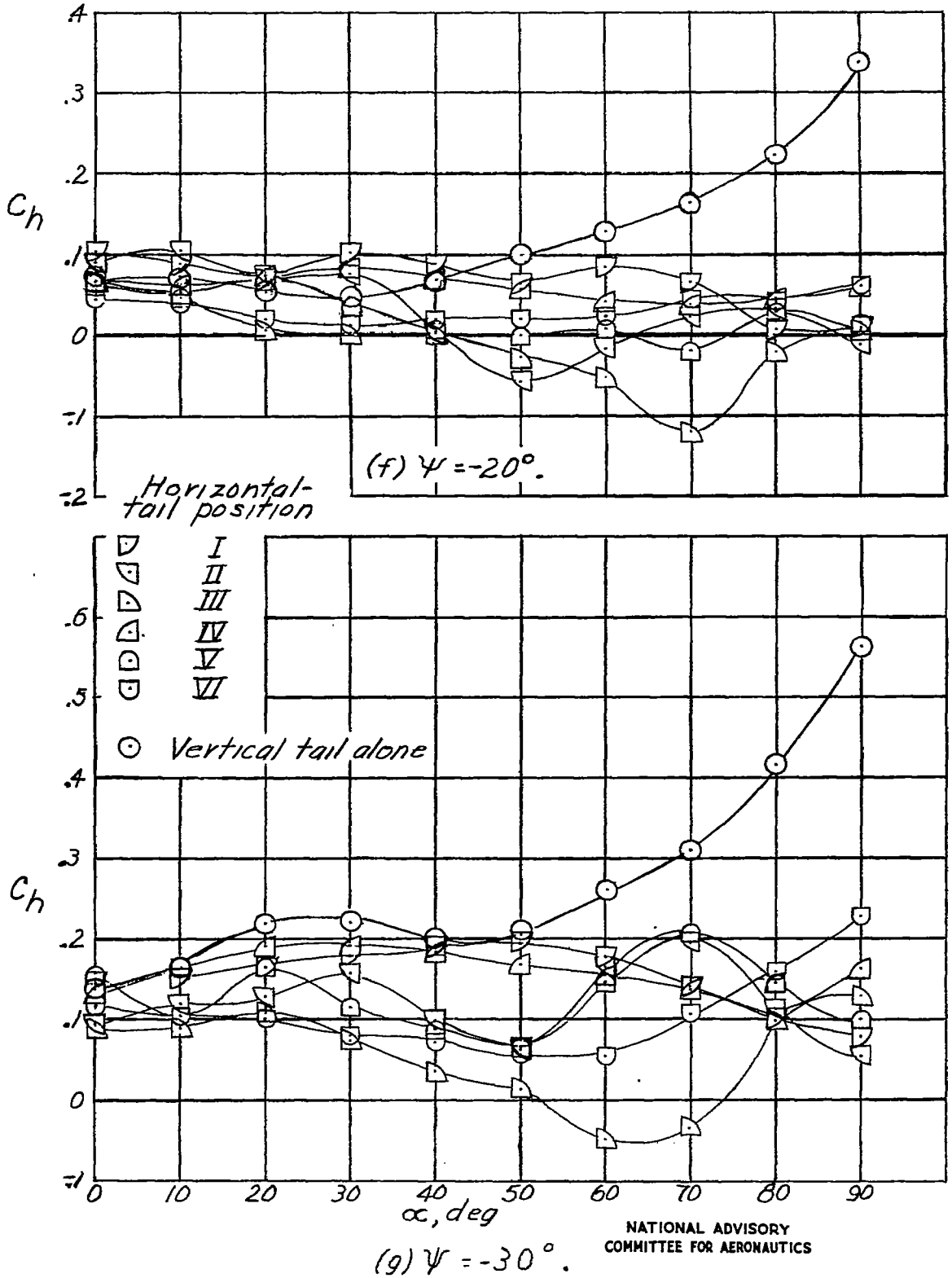

Figure 7.- Concluded.

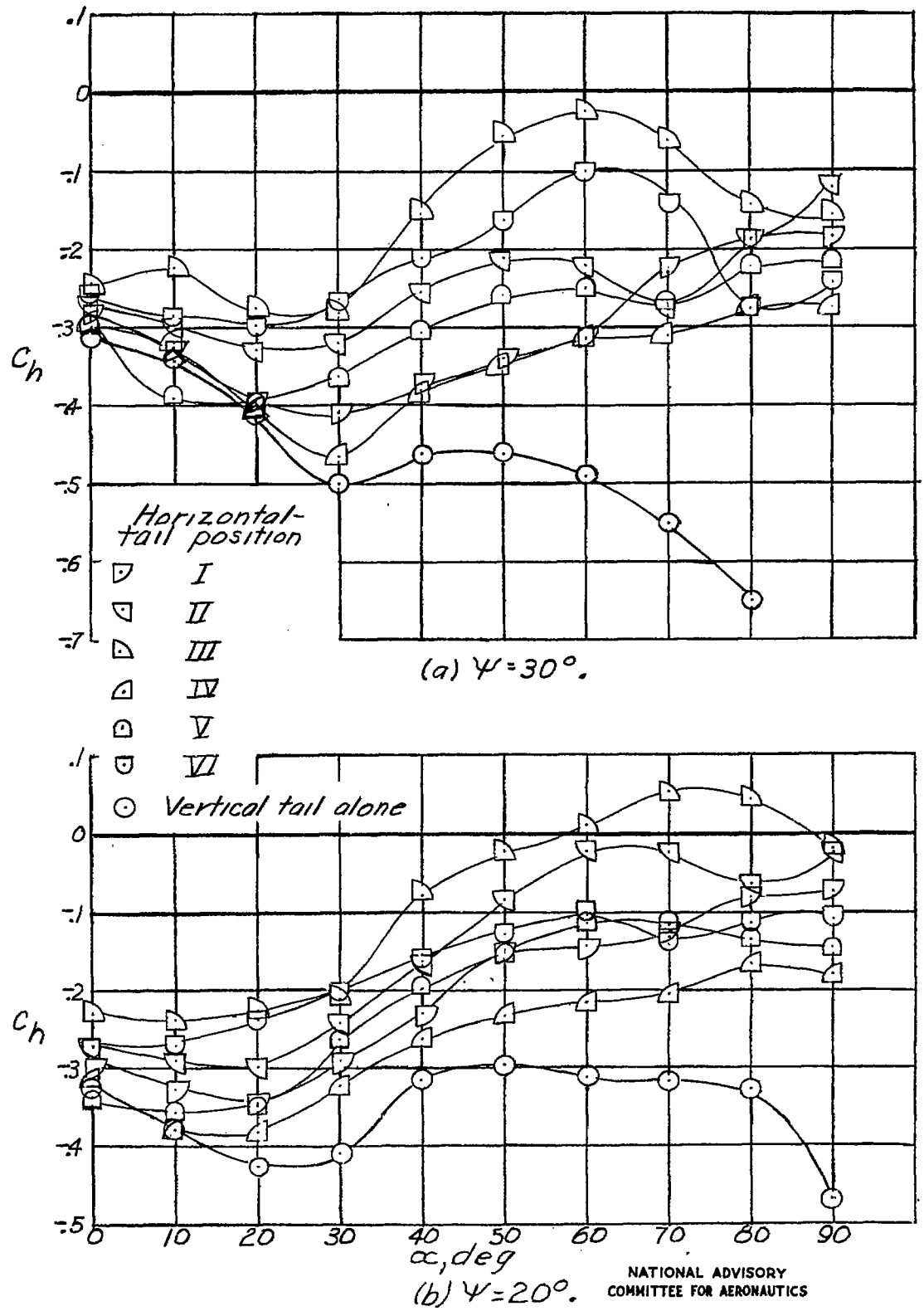

Figure 8.- Rudder hinge-moment coefficient as a function of angle of attack at $\delta_r = 20°$ for various angles of yaw and positions of horizontal tail.

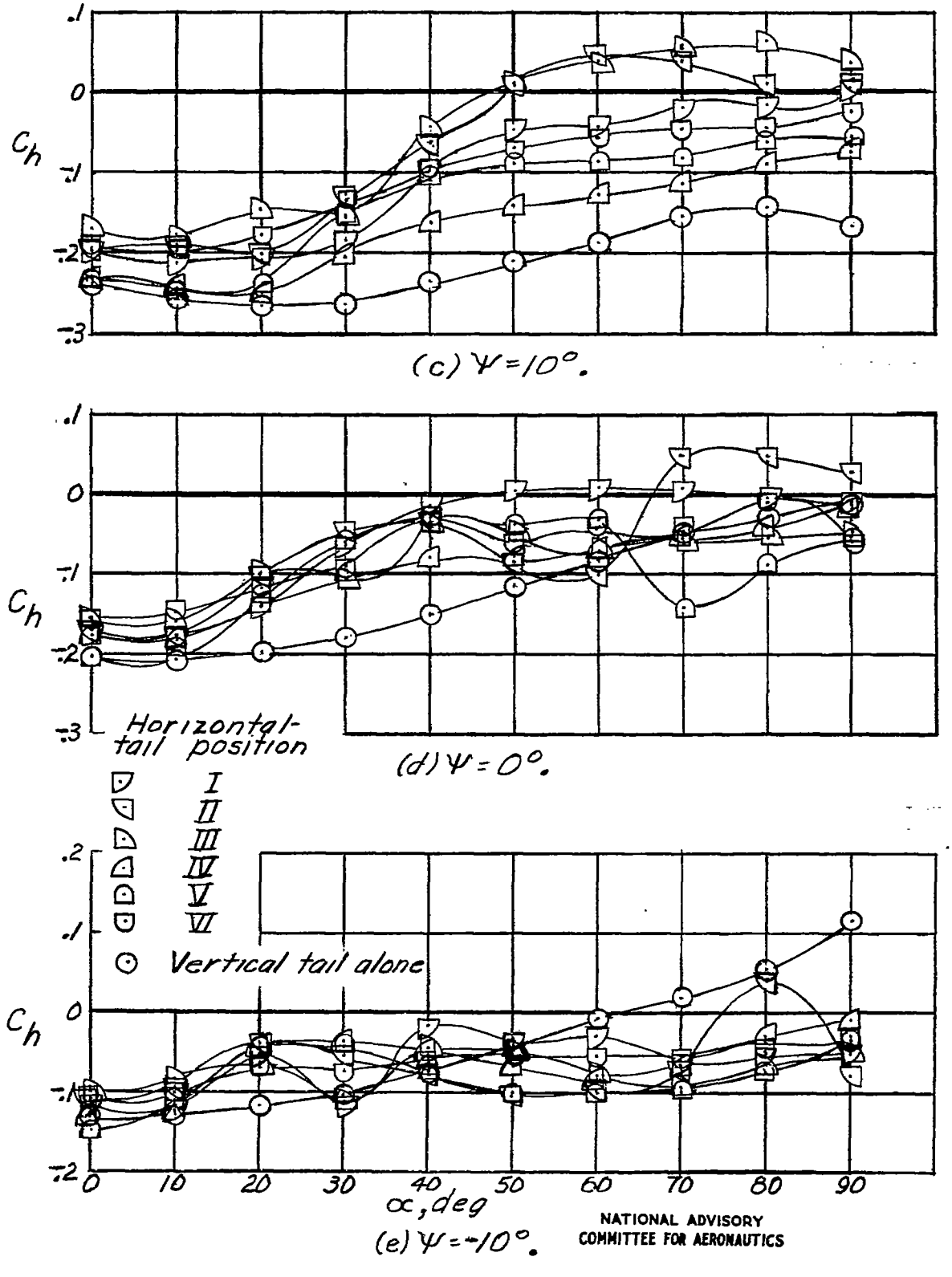

Figure 8.- Continued.

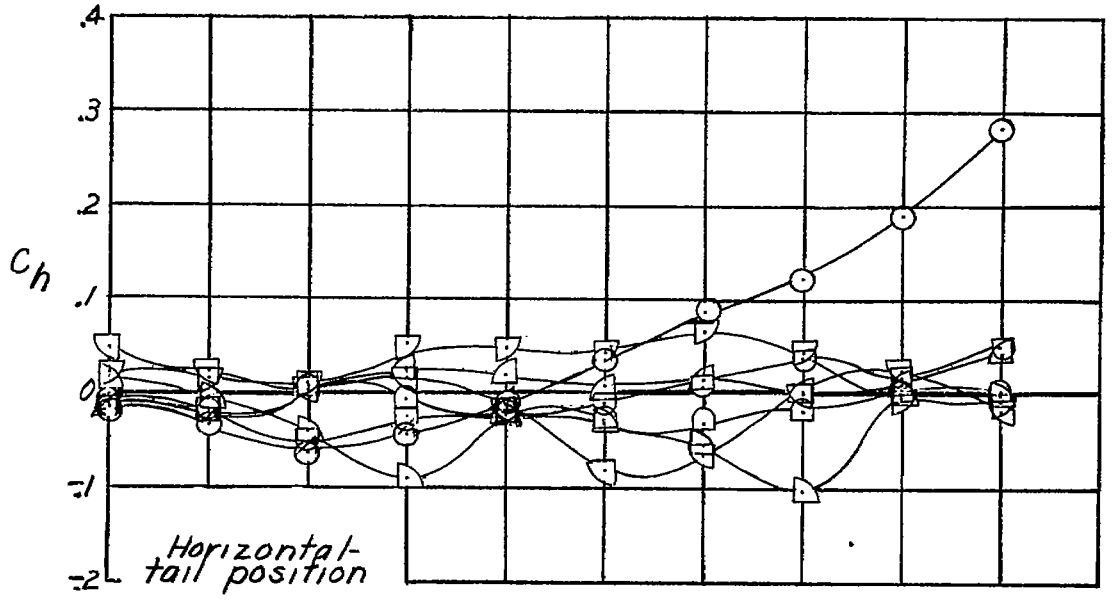

(f) $\Psi = -20°$.

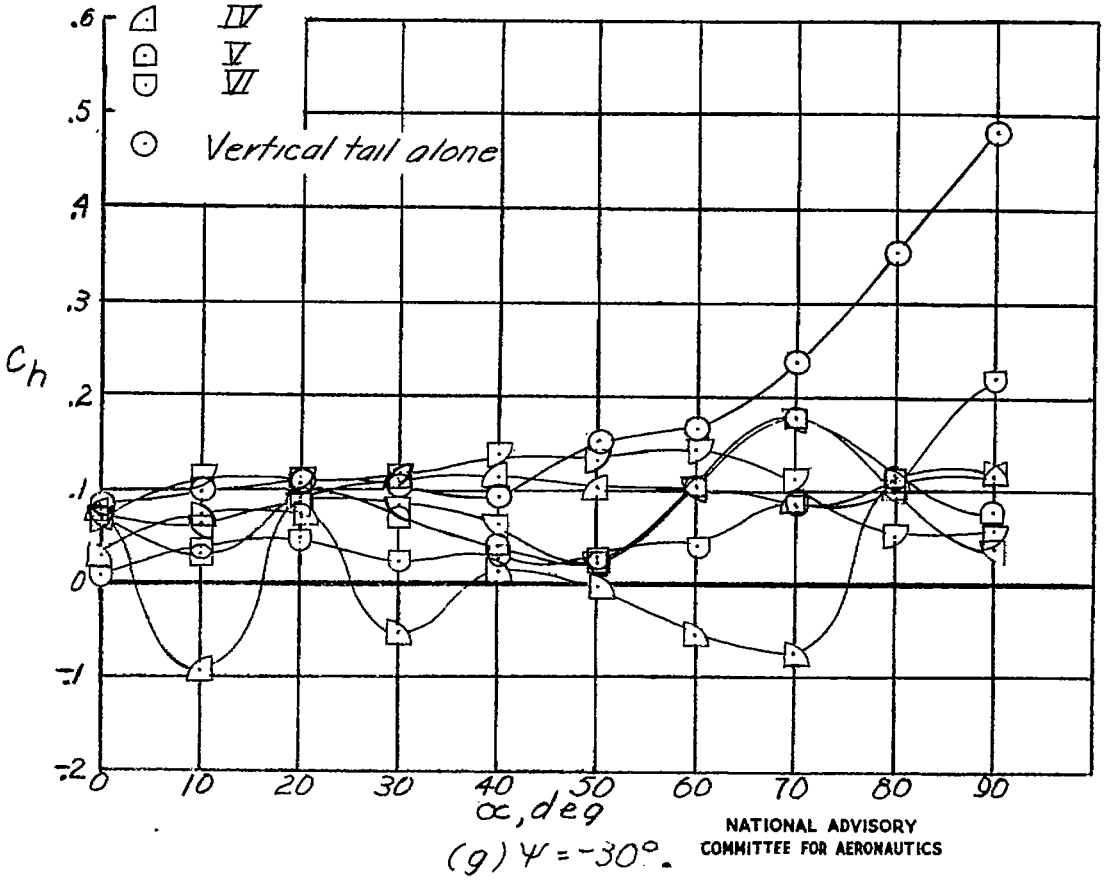

(g) $\Psi = -30°$.

Figure 8.- Concluded.

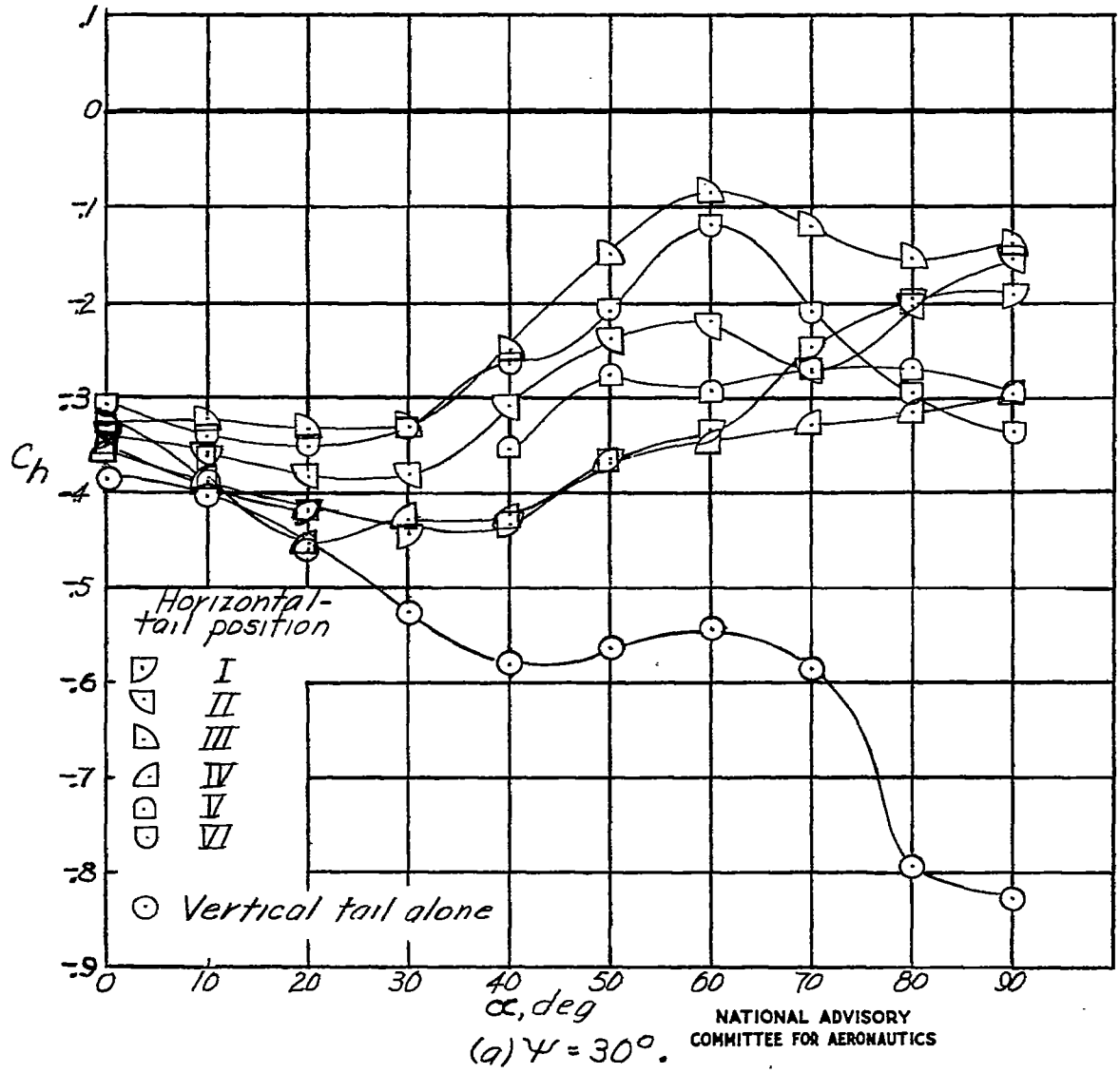

Figure 9.- Rudder hinge-moment coefficient as a function of angle of attack at $\delta_r = 30^\circ$ for various angles of yaw and positions of horizontal tail.

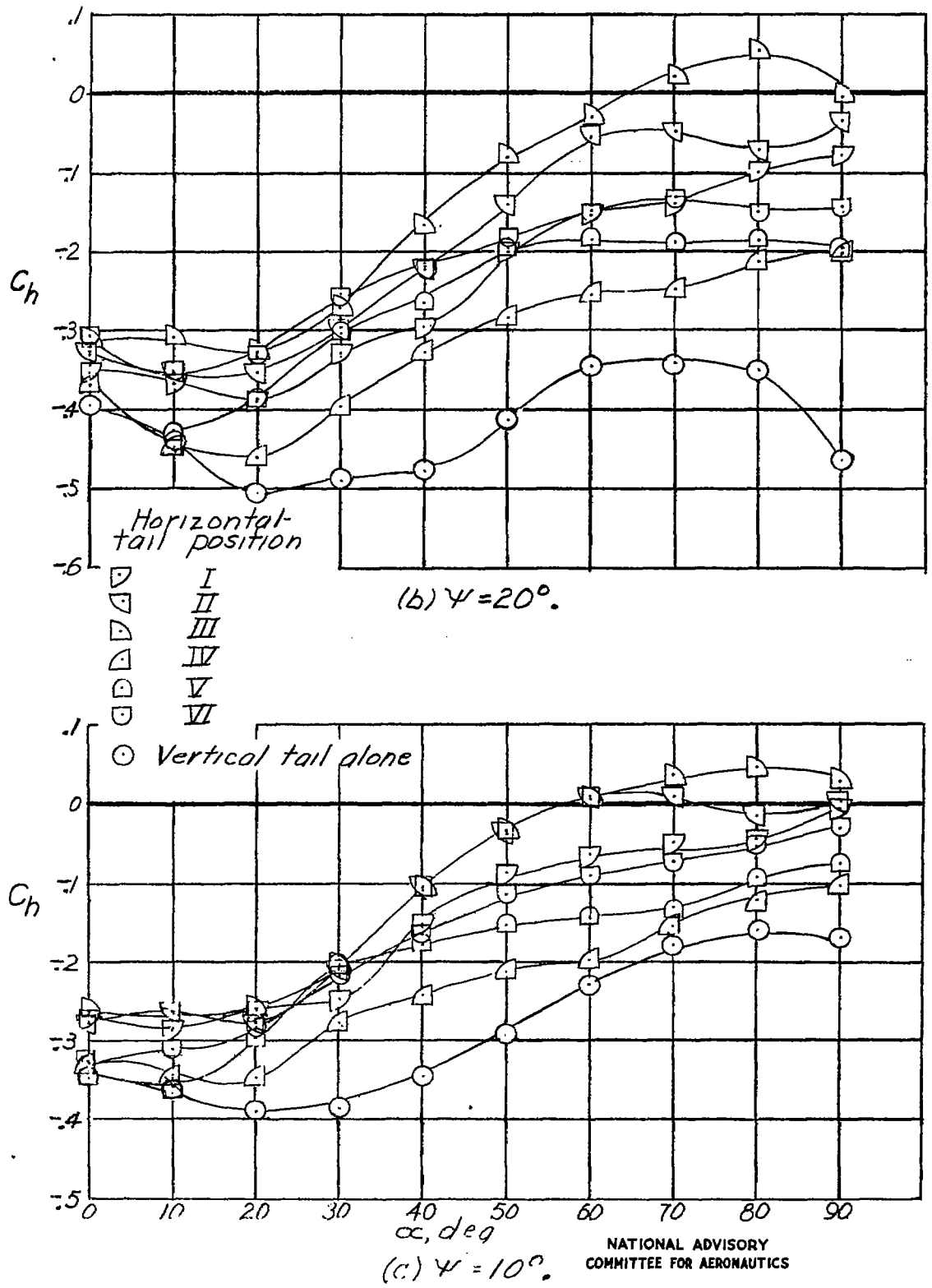

Figure 9.- Continued.

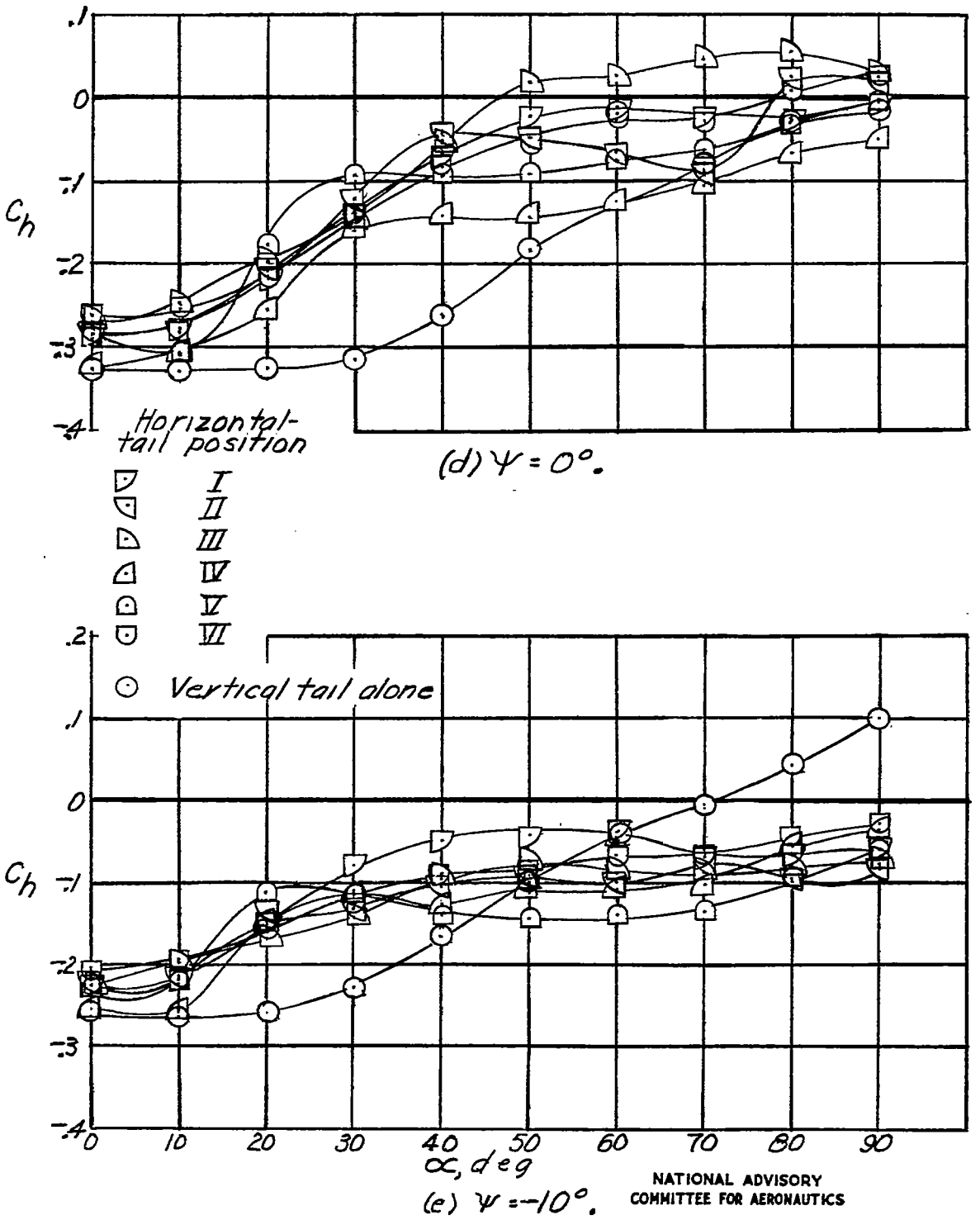

Figure 9.- Continued.

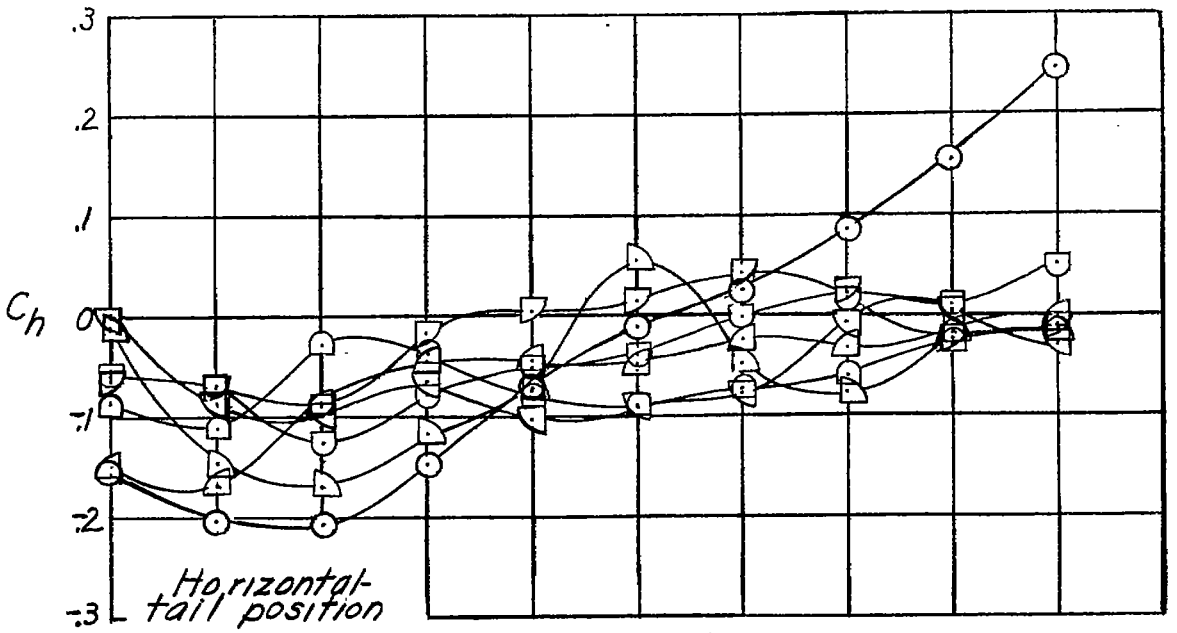

(f) $\psi = -20°$.

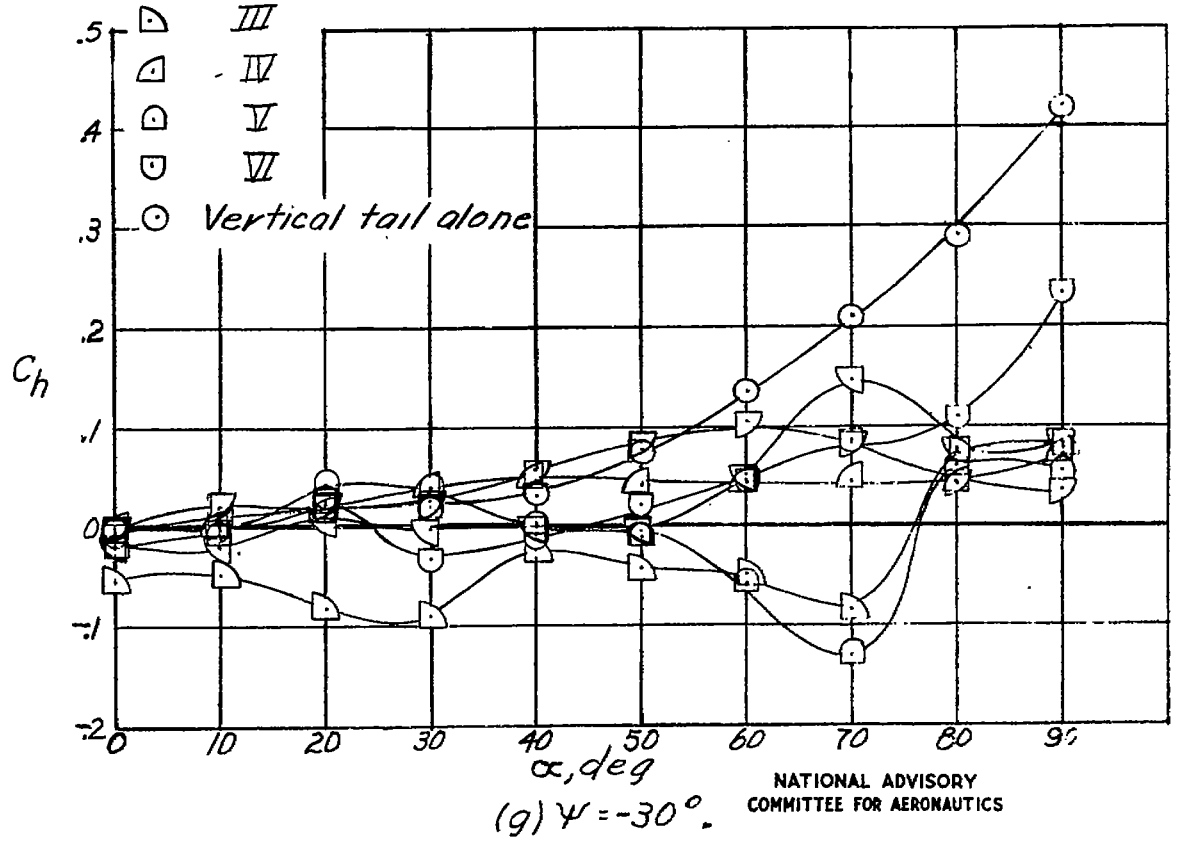

(g) $\psi = -30°$.

Figure 9.- Concluded.

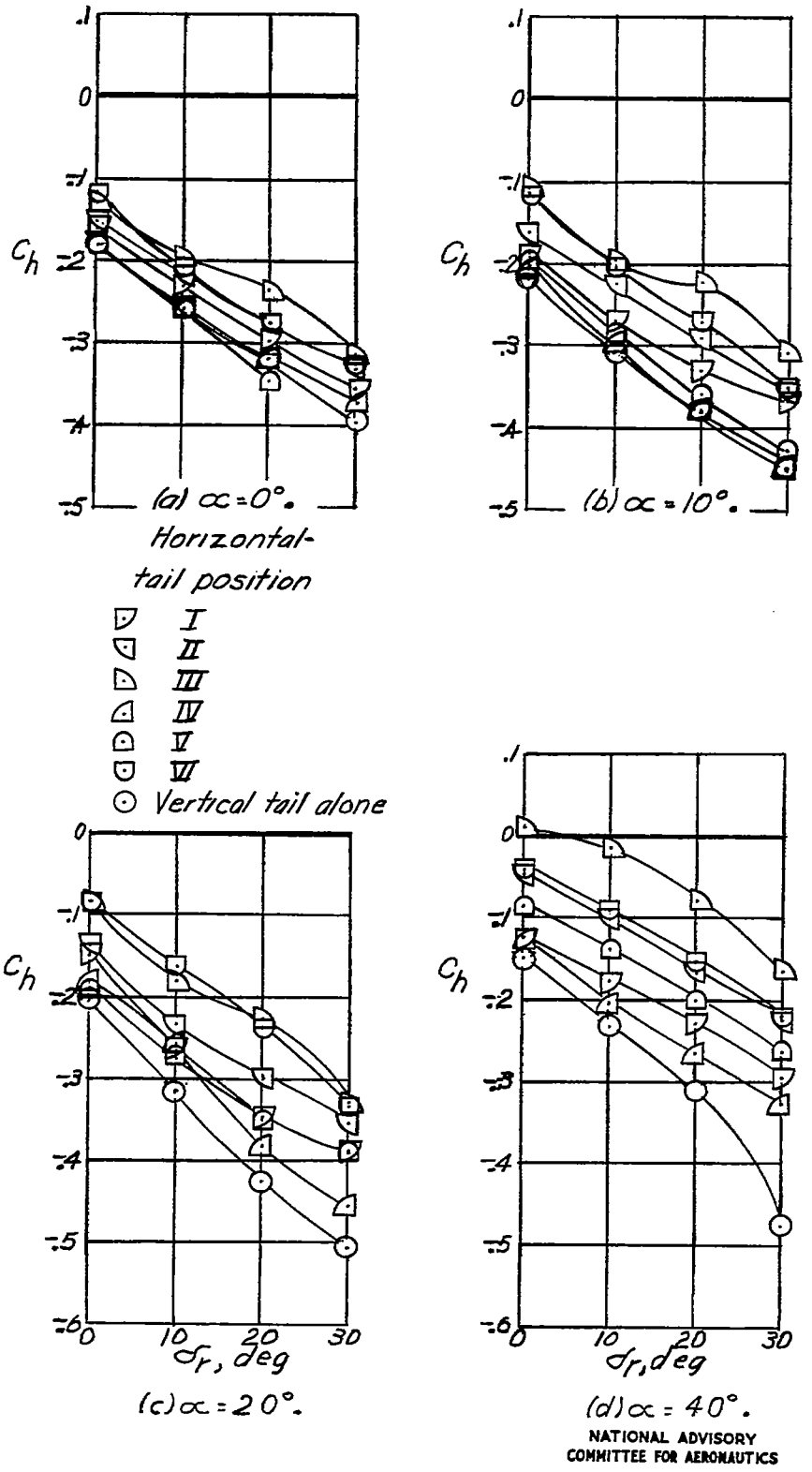

Figure 10.- Rudder hinge-moment coefficient as a function of rudder deflection at $\psi = 20°$ for various angles of attack and positions of horizontal tail.

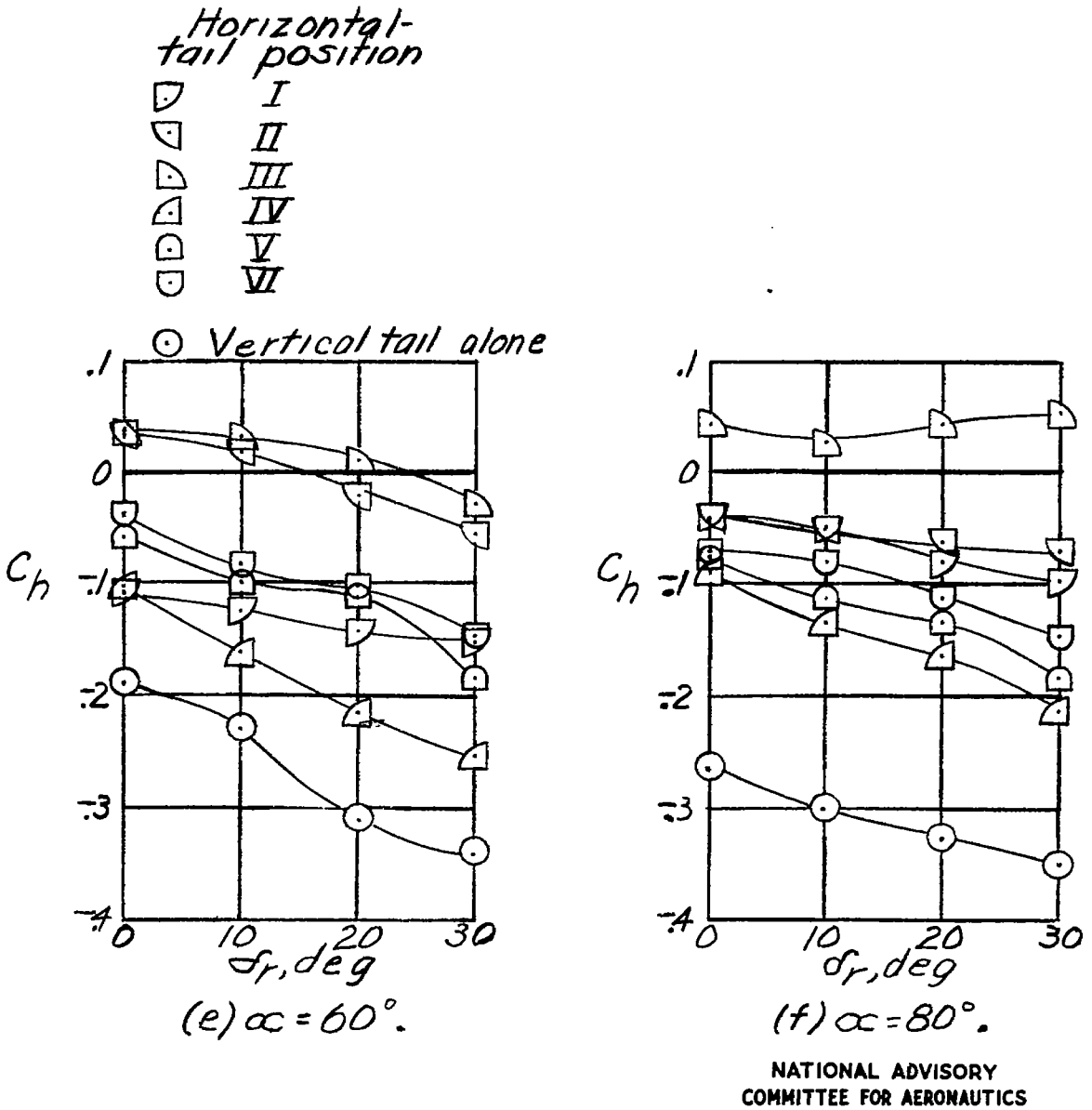

Figure 10.- Concluded.

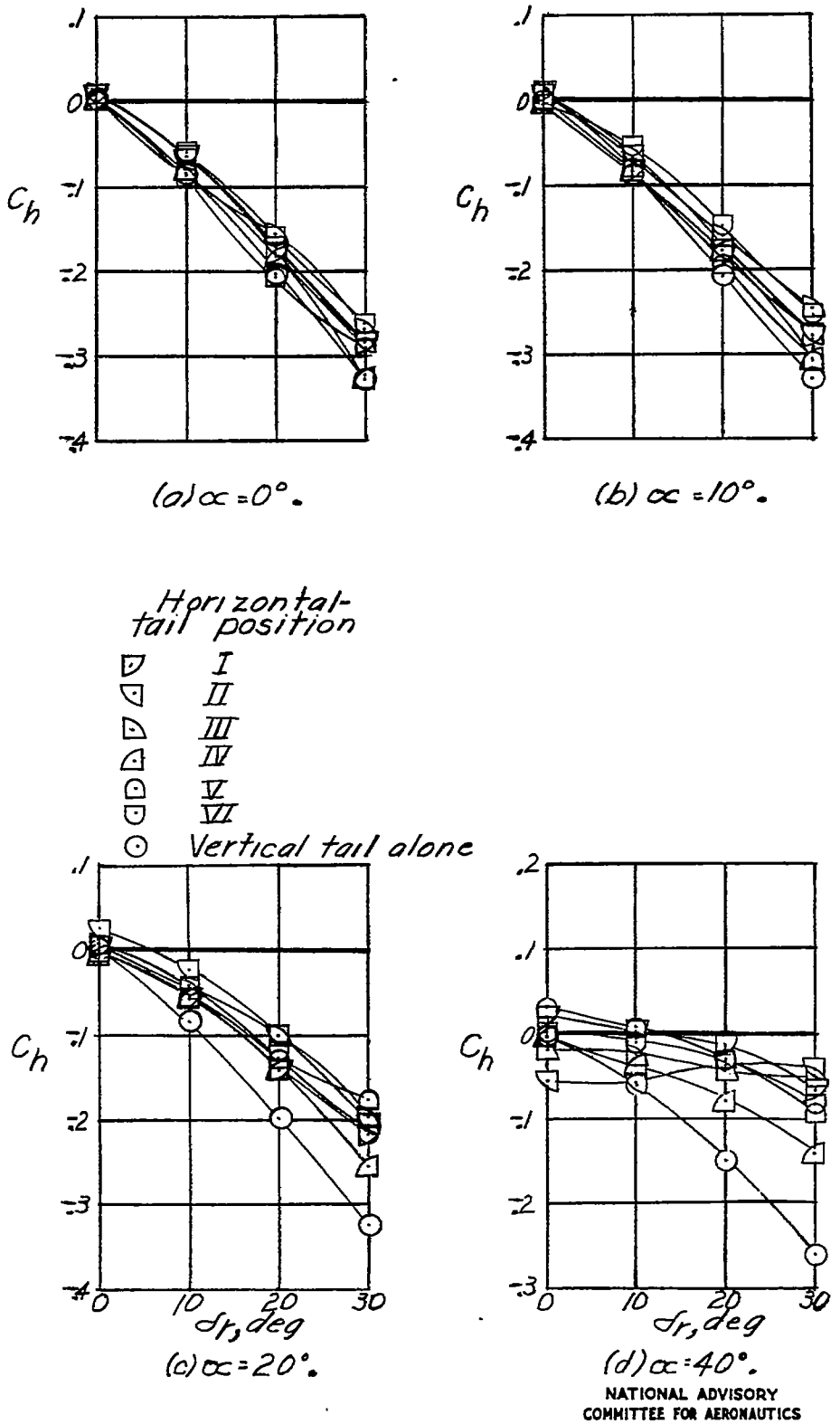

Figure 11.- Rudder hinge-moment coefficient as a function of rudder deflection at $\psi = 0°$ for various angles of attack and positions of horizontal tail.

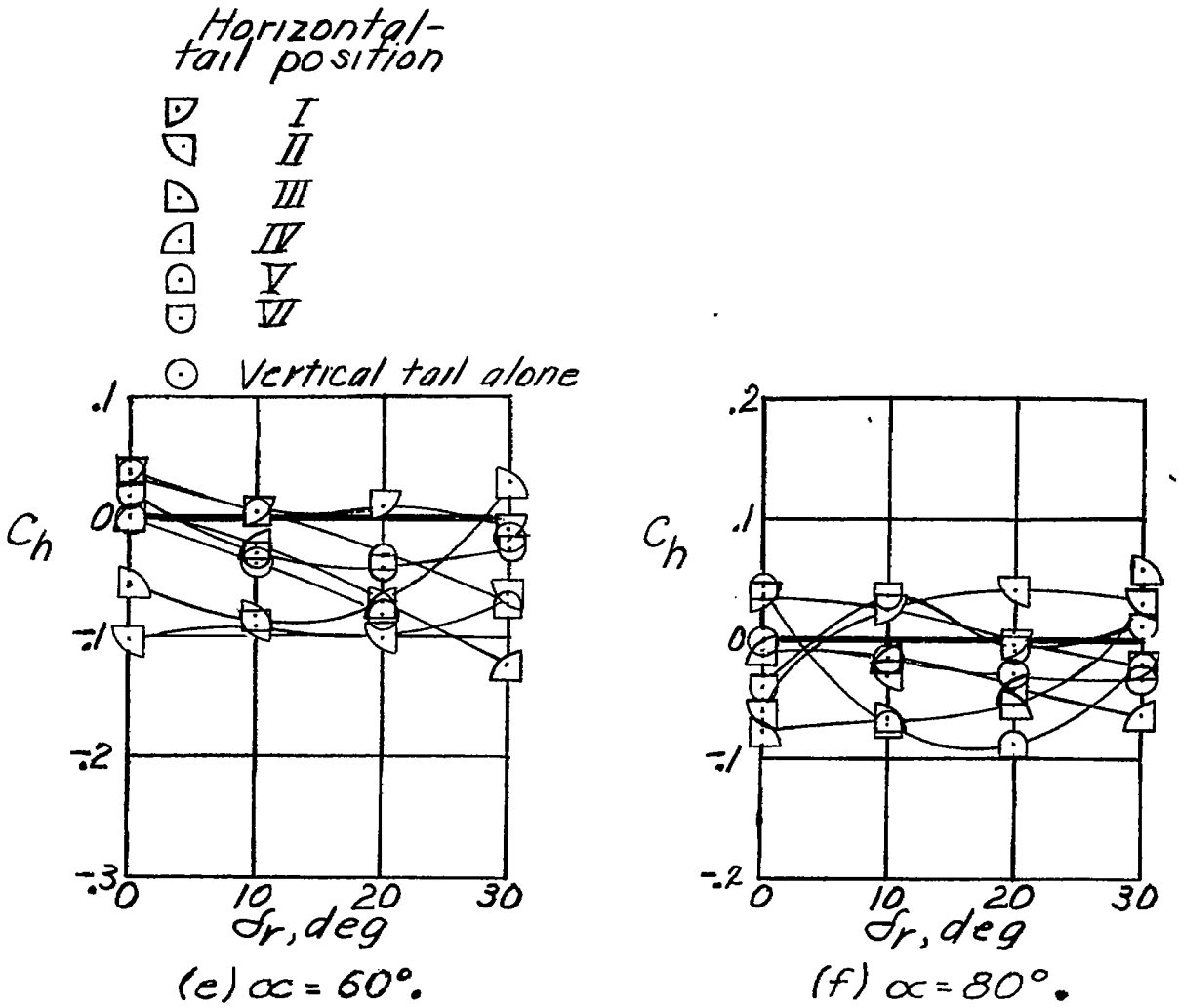

Figure 11.- Concluded.

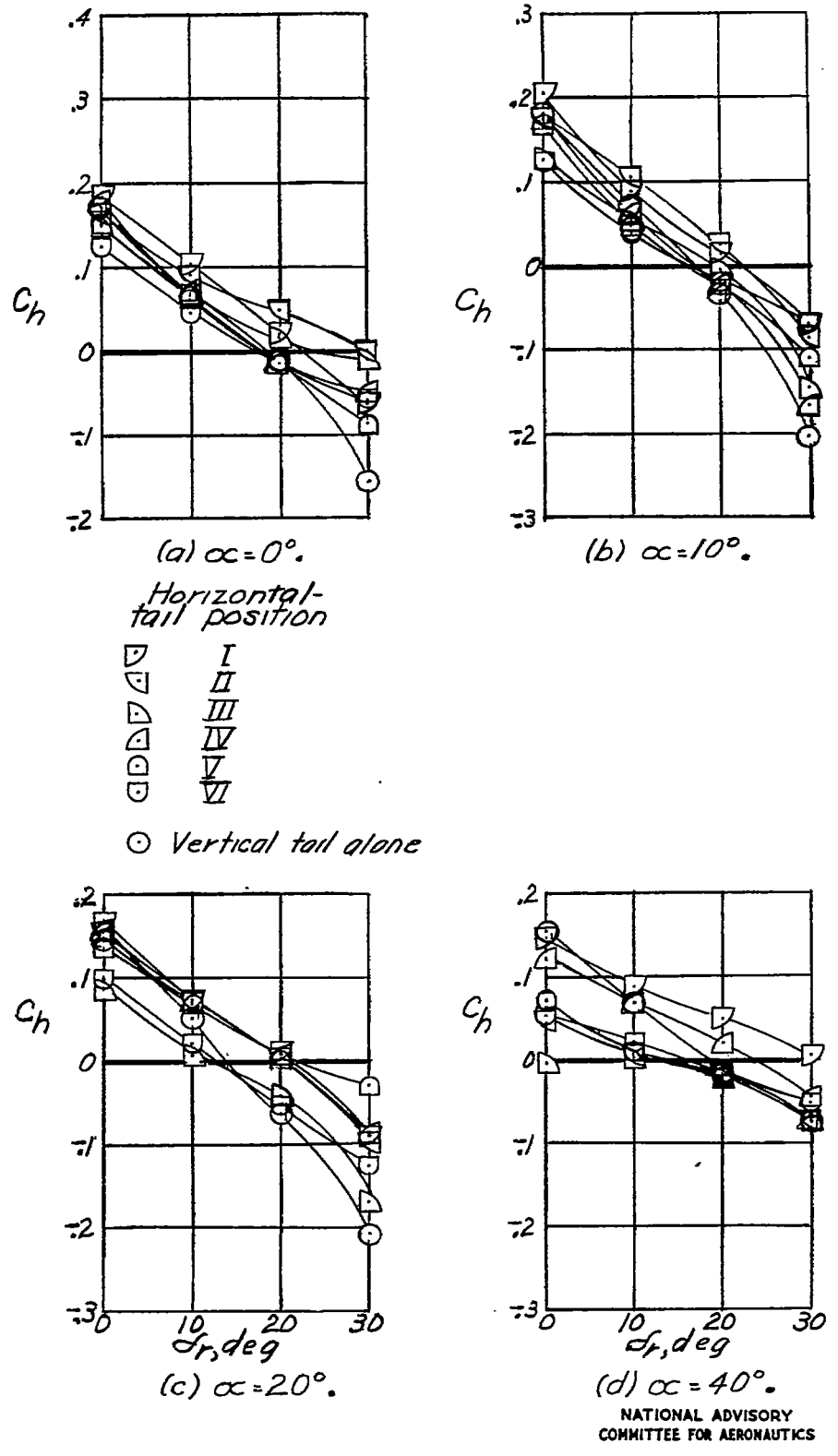

Figure 12.- Rudder hinge-moment coefficient as a function of rudder deflection at $\psi = -20°$ for various angles of attack and positions of horizontal tail.

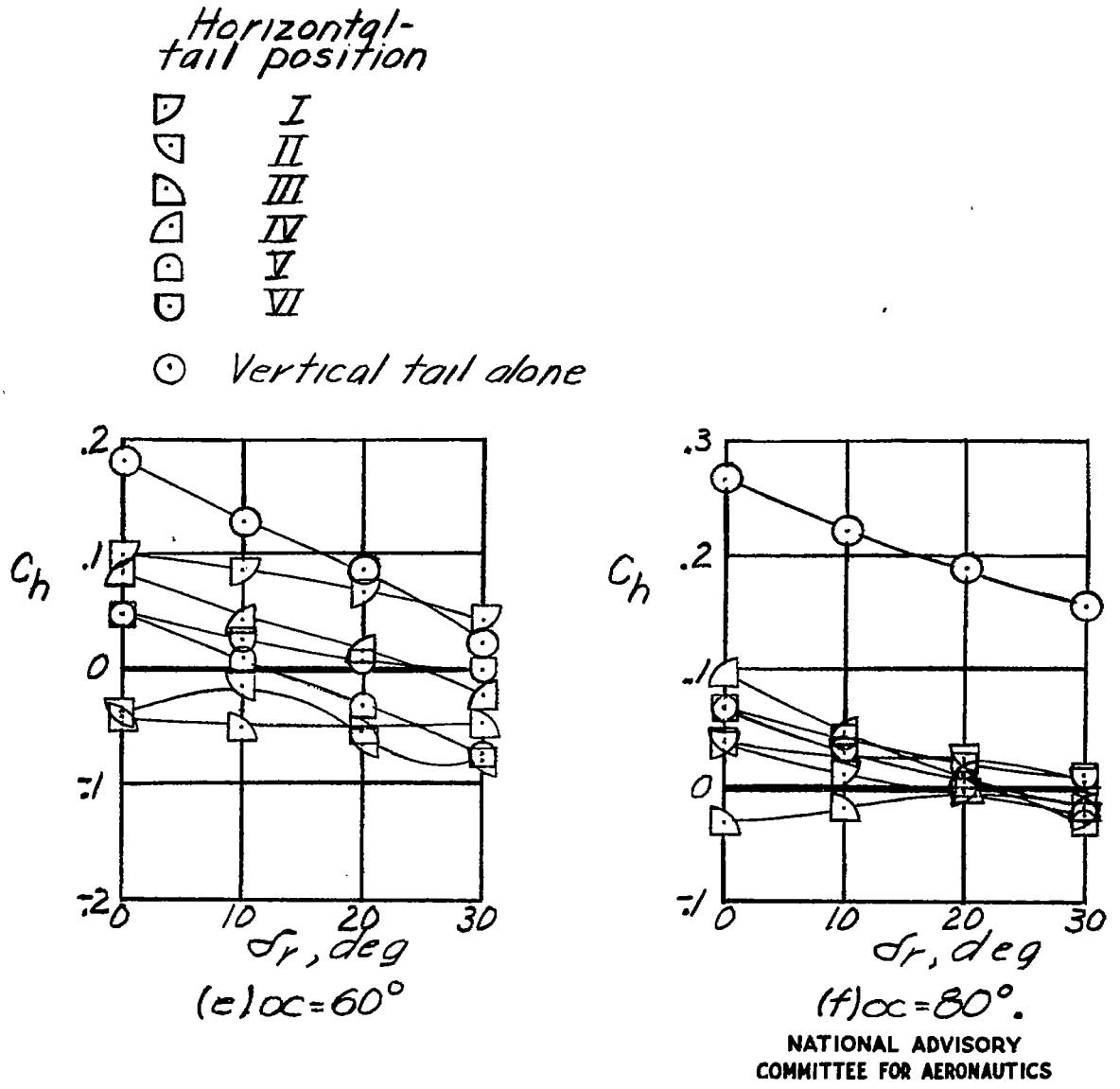

Figure 12.- Concluded.

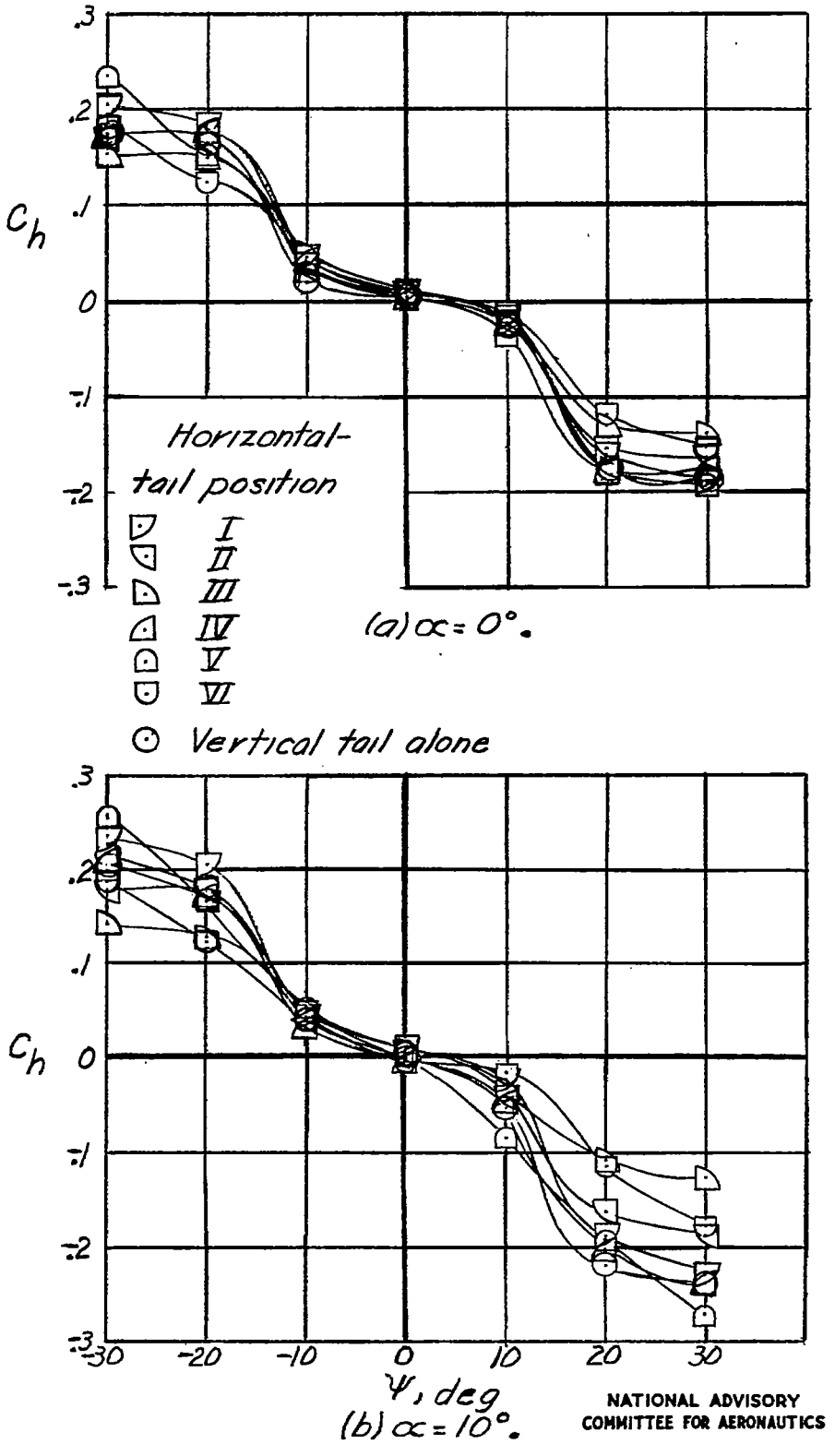

Figure 13.- Rudder hinge-moment coefficient as a function of angle of yaw at $\delta_r = 0°$ for various angles of attack and positions of horizontal tail.

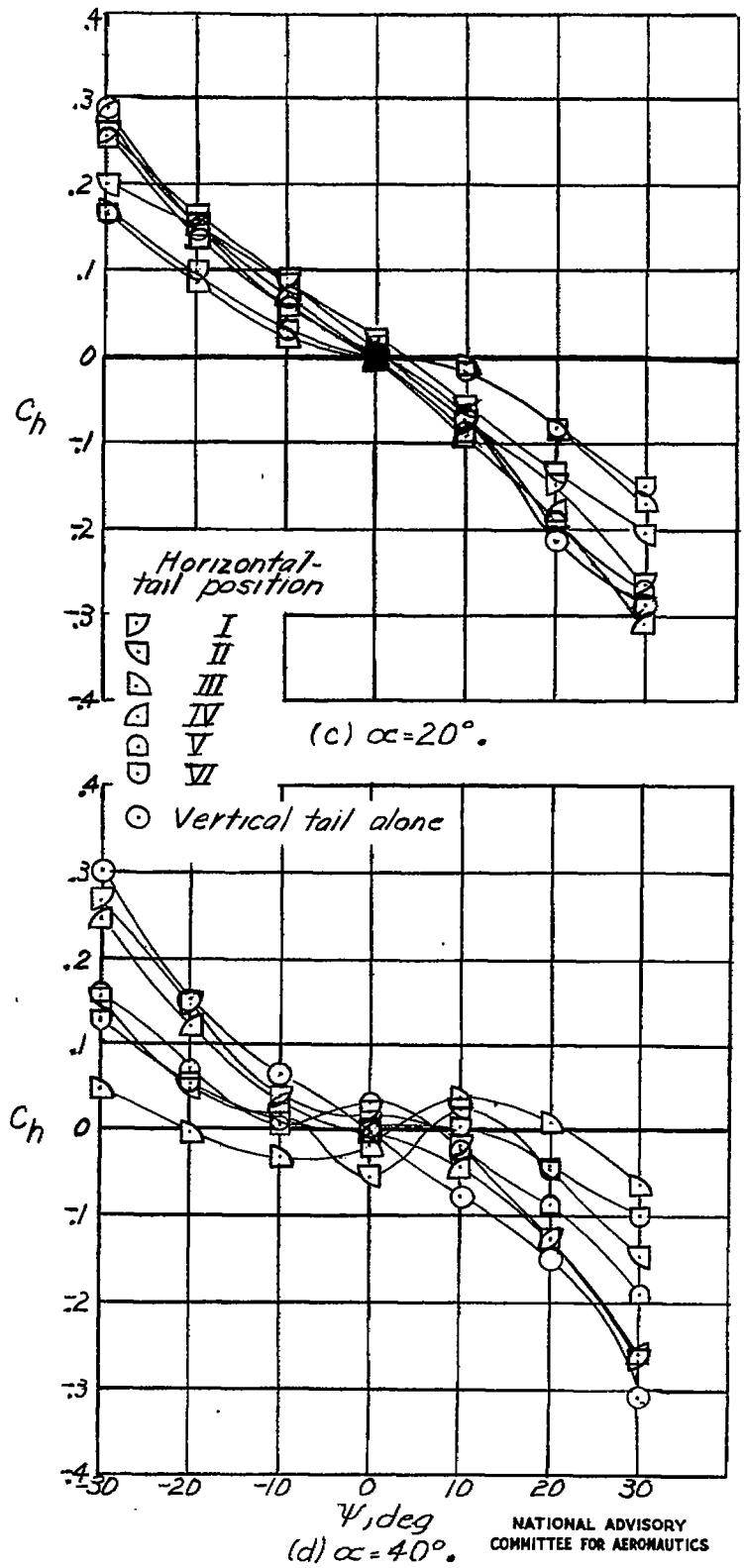

Figure 13.- Continued.

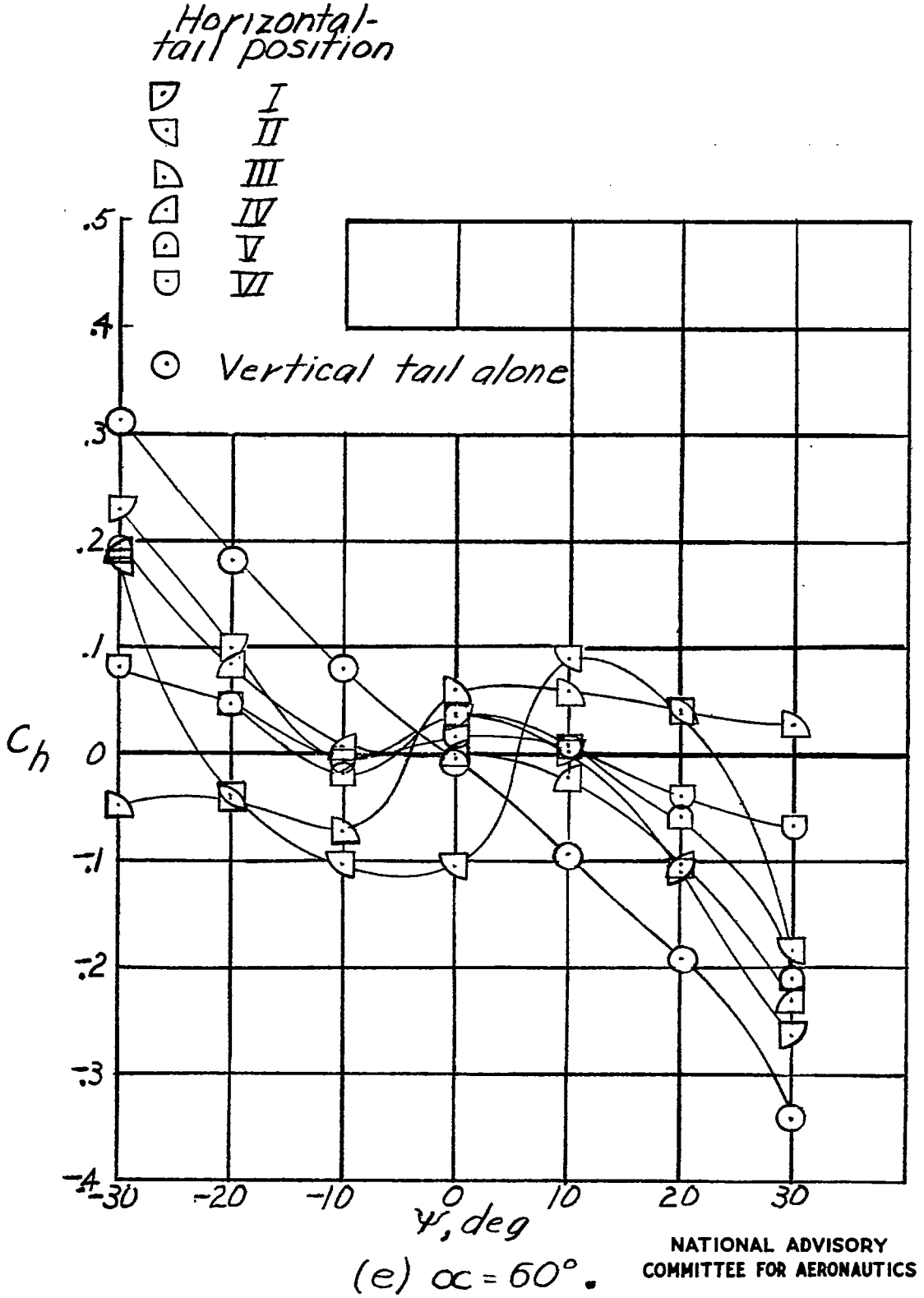

Figure 13.- Continued.

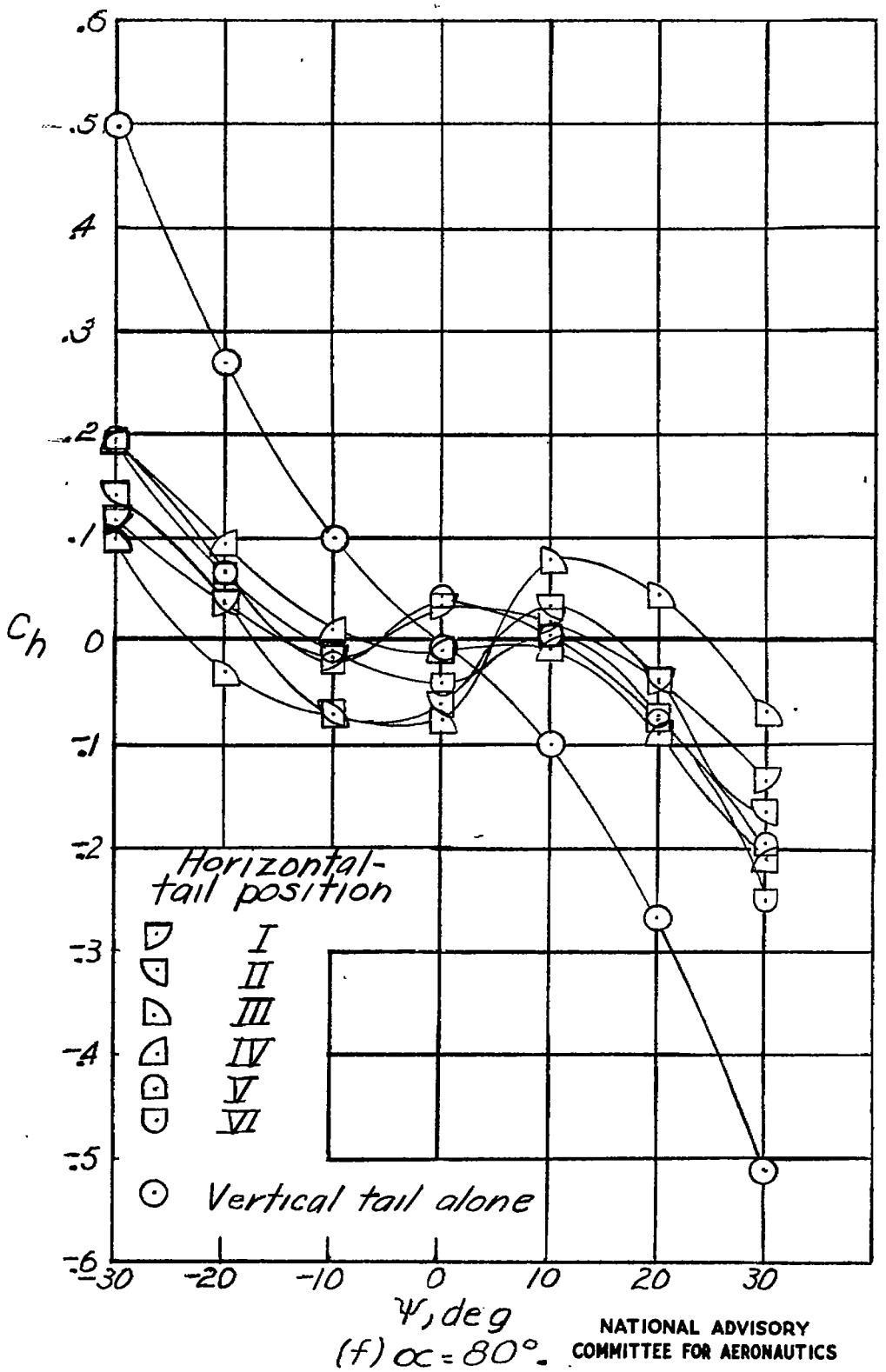

Figure 13.- Concluded.

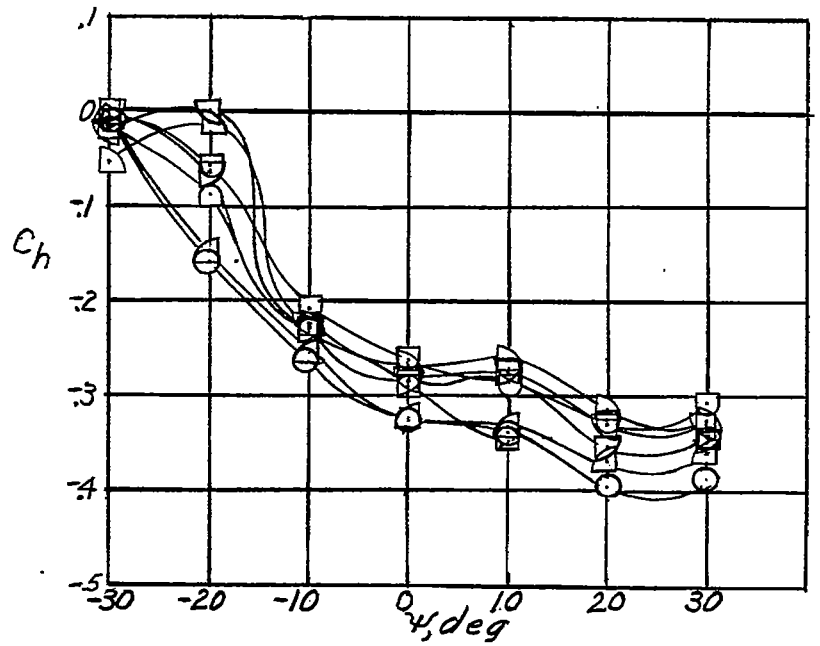

(a) $\alpha = 0°$.

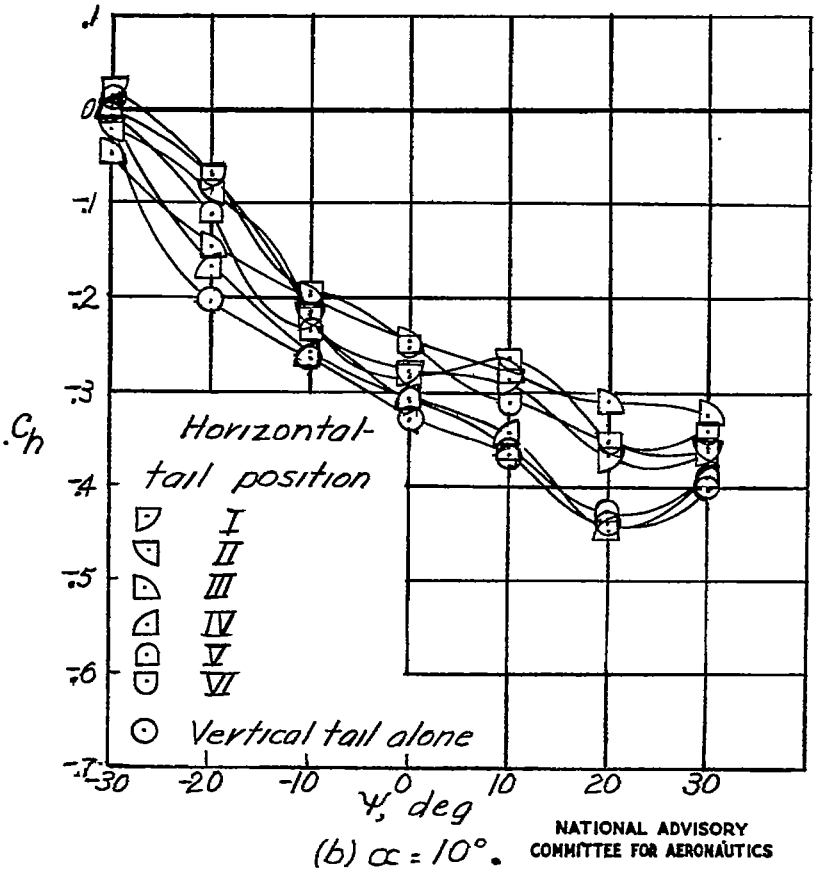

(b) $\alpha = 10°$.

Figure 14.- Rudder hinge-moment coefficient as a function of angle of yaw at $\delta_r = 30°$ for various angles of attack and positions of horizontal tail.

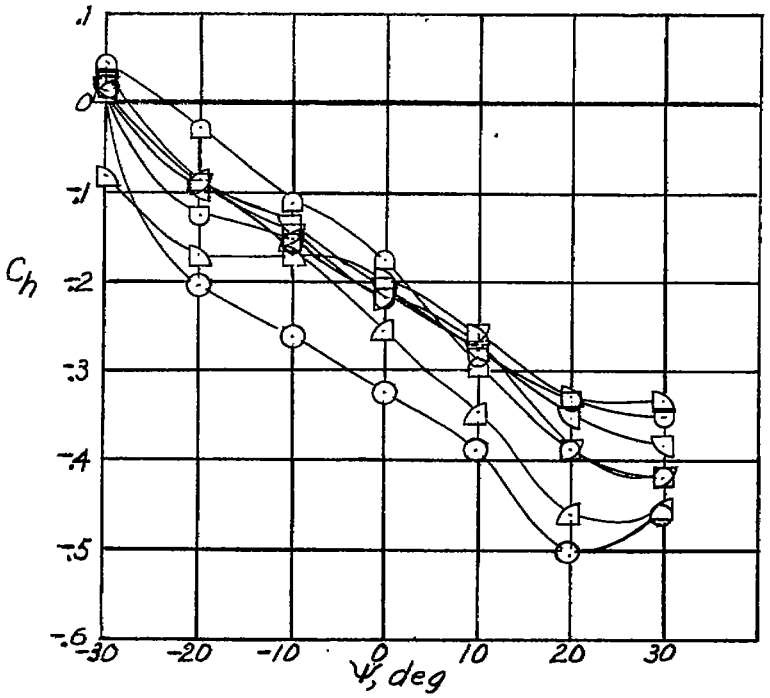

(c) $\alpha = 20°$.

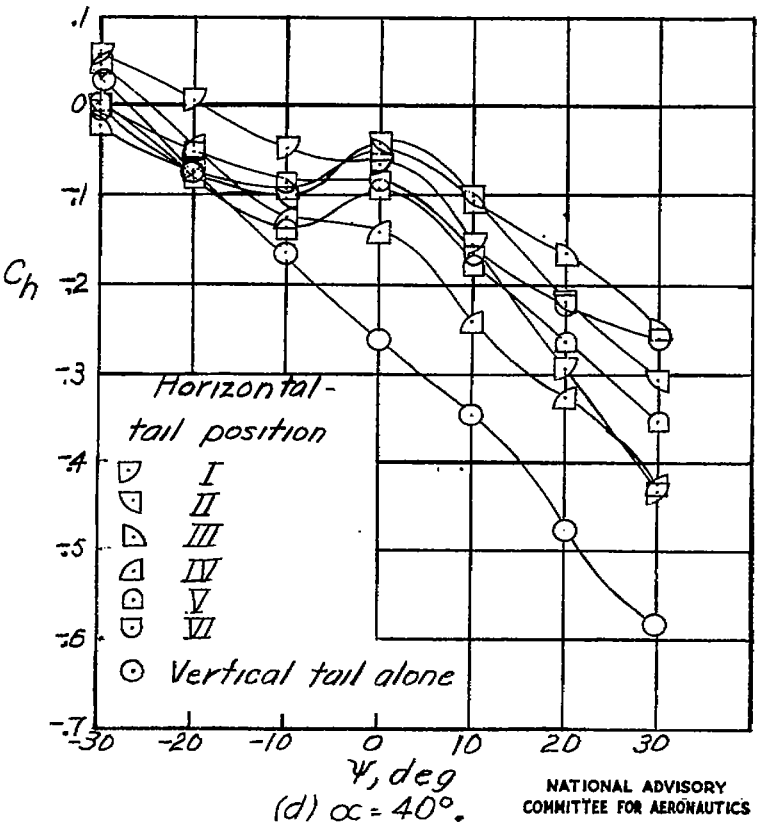

(d) $\alpha = 40°$.

Figure 14.- Continued.

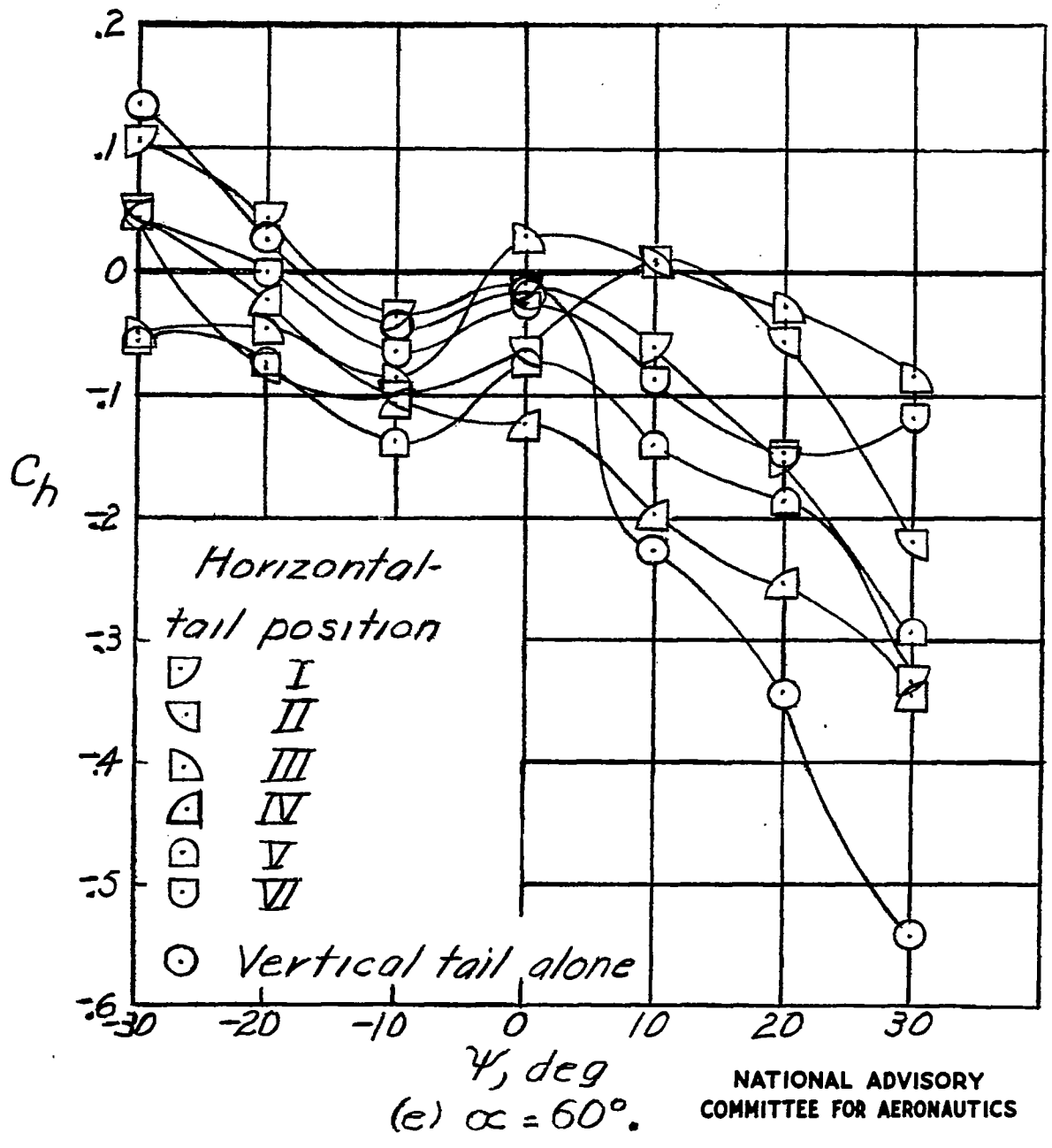

Figure 14.- Continued.

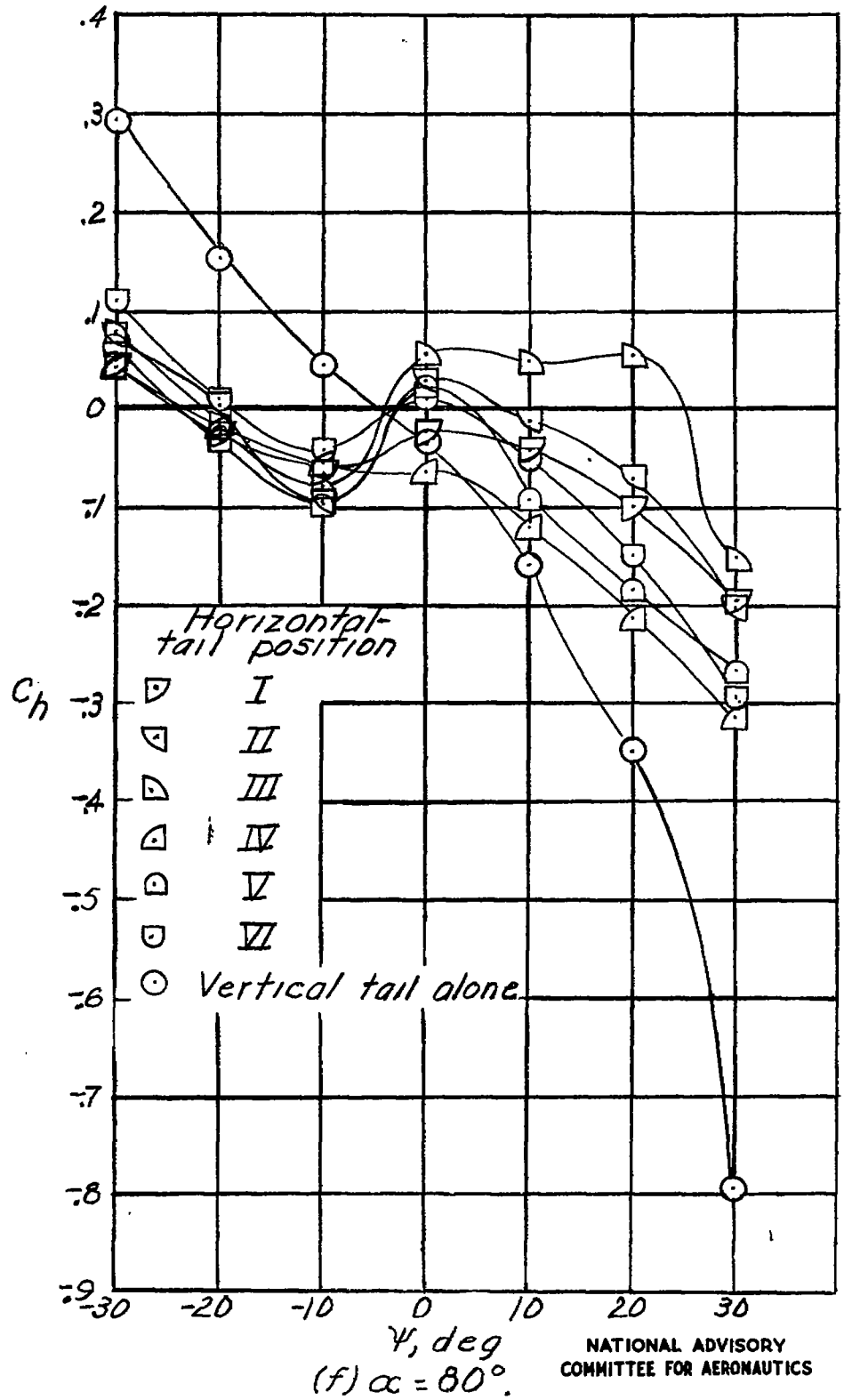

Figure 14.- Concluded.

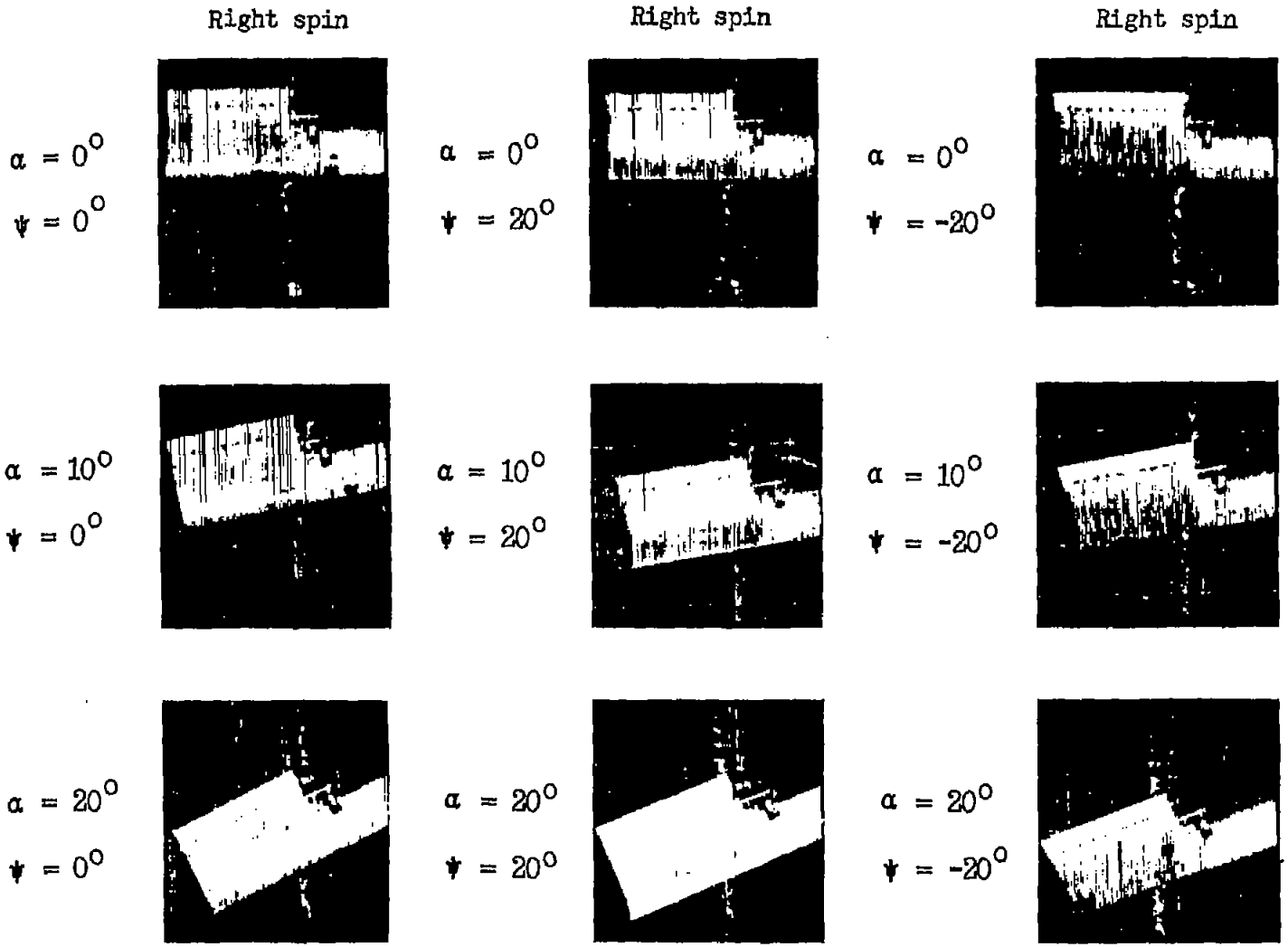

Figure 15.- Photographs of tuft tests performed on vertical tail alone in Langley 15-foot free-spinning tunnel.

NATIONAL ADVISORY COMMITTEE FOR AERONAUTICS
LANGLEY MEMORIAL AERONAUTICAL LABORATORY - LANGLEY FIELD VA

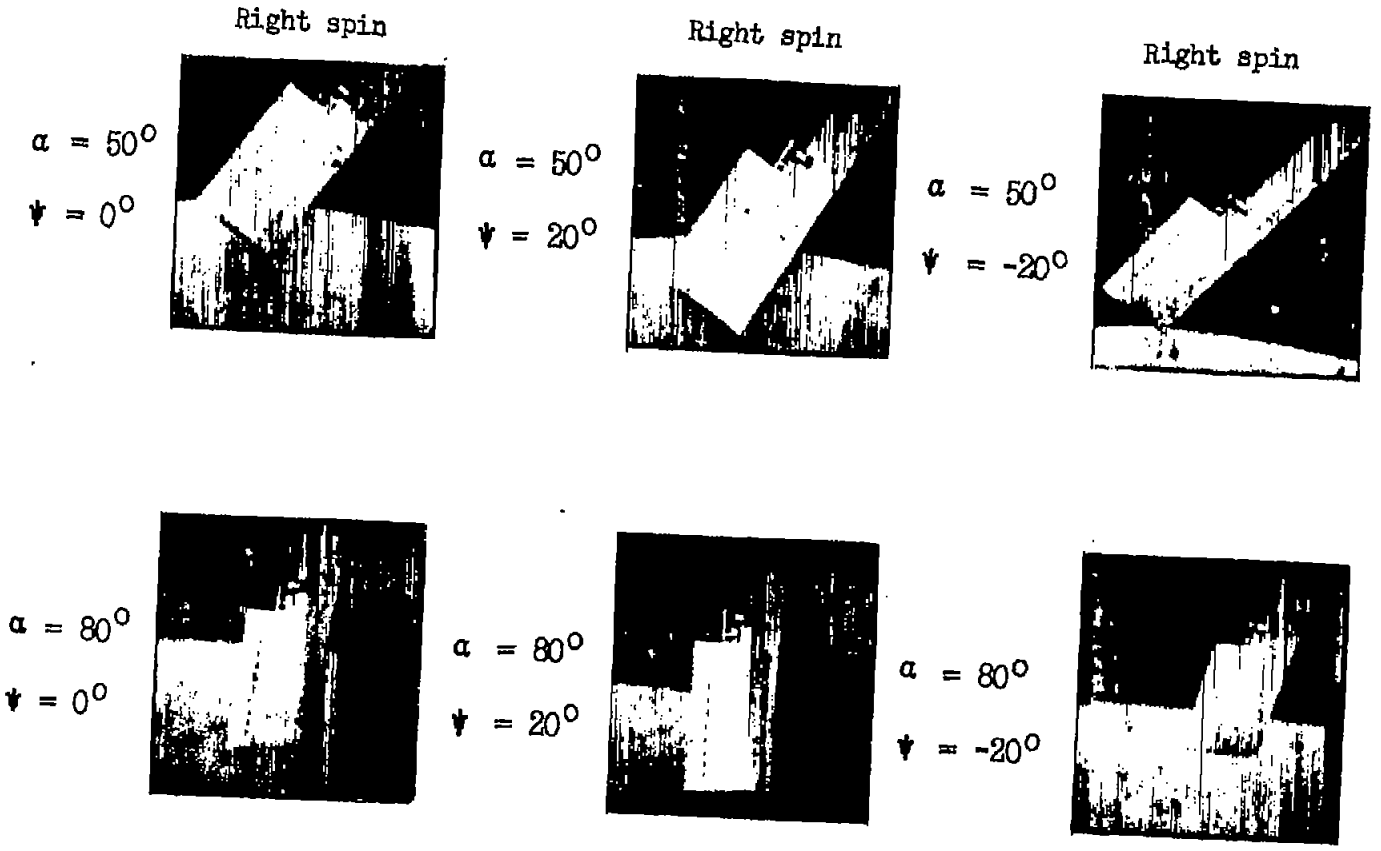

Figure 15.- Concluded.

NATIONAL ADVISORY COMMITTEE FOR AERONAUTICS
LANGLEY MEMORIAL AERONAUTICAL LABORATORY - LANGLEY FIELD, VA

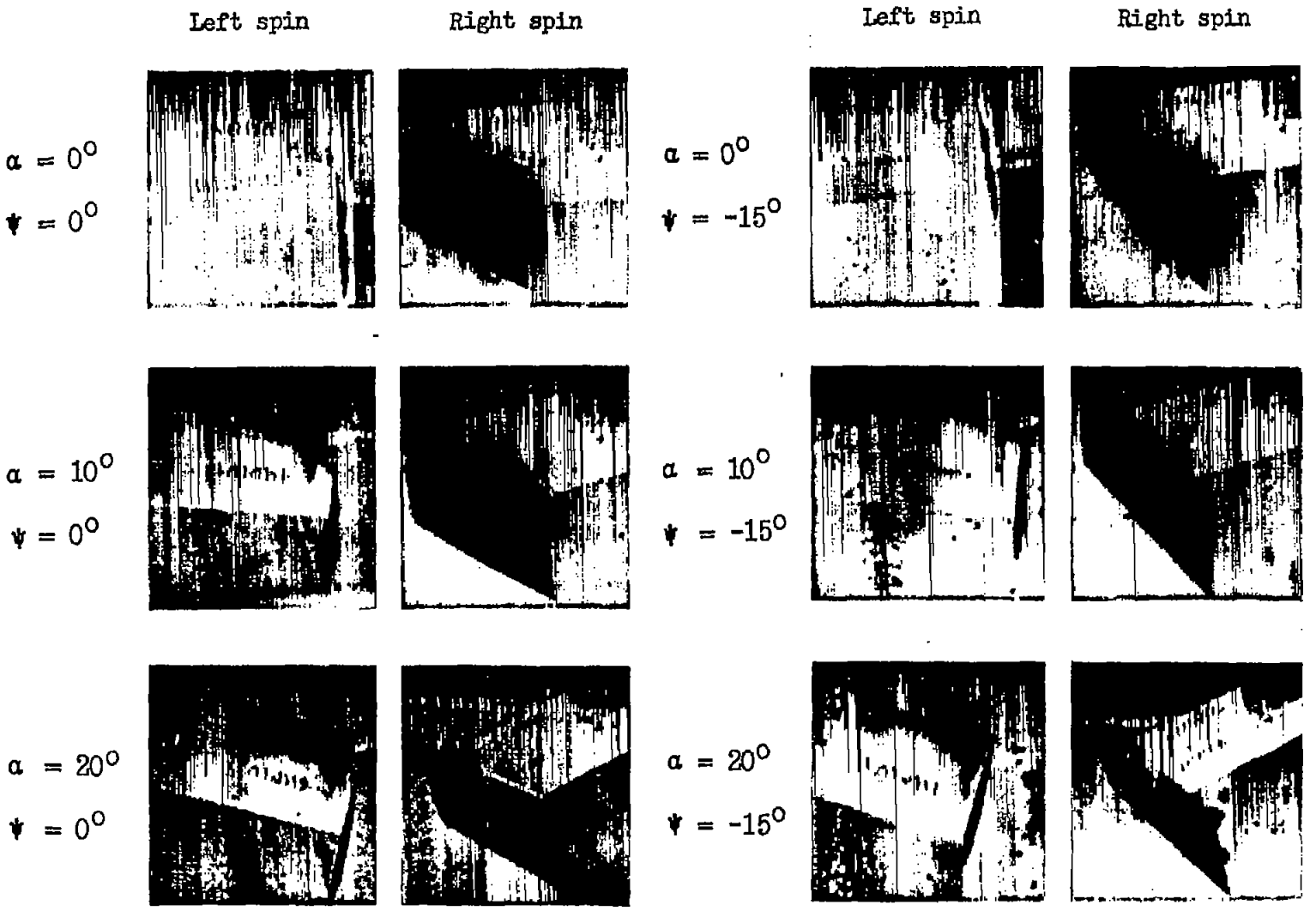

Figure 16.- Photographs of tuft tests performed on vertical tail in combination with horizontal tail in Langley 15-foot free-spinning tunnel. Horizontal tail is in position I.

NATIONAL ADVISORY COMMITTEE FOR AERONAUTICS
LANGLEY MEMORIAL AERONAUTICAL LABORATORY - LANGLEY FIELD, VA

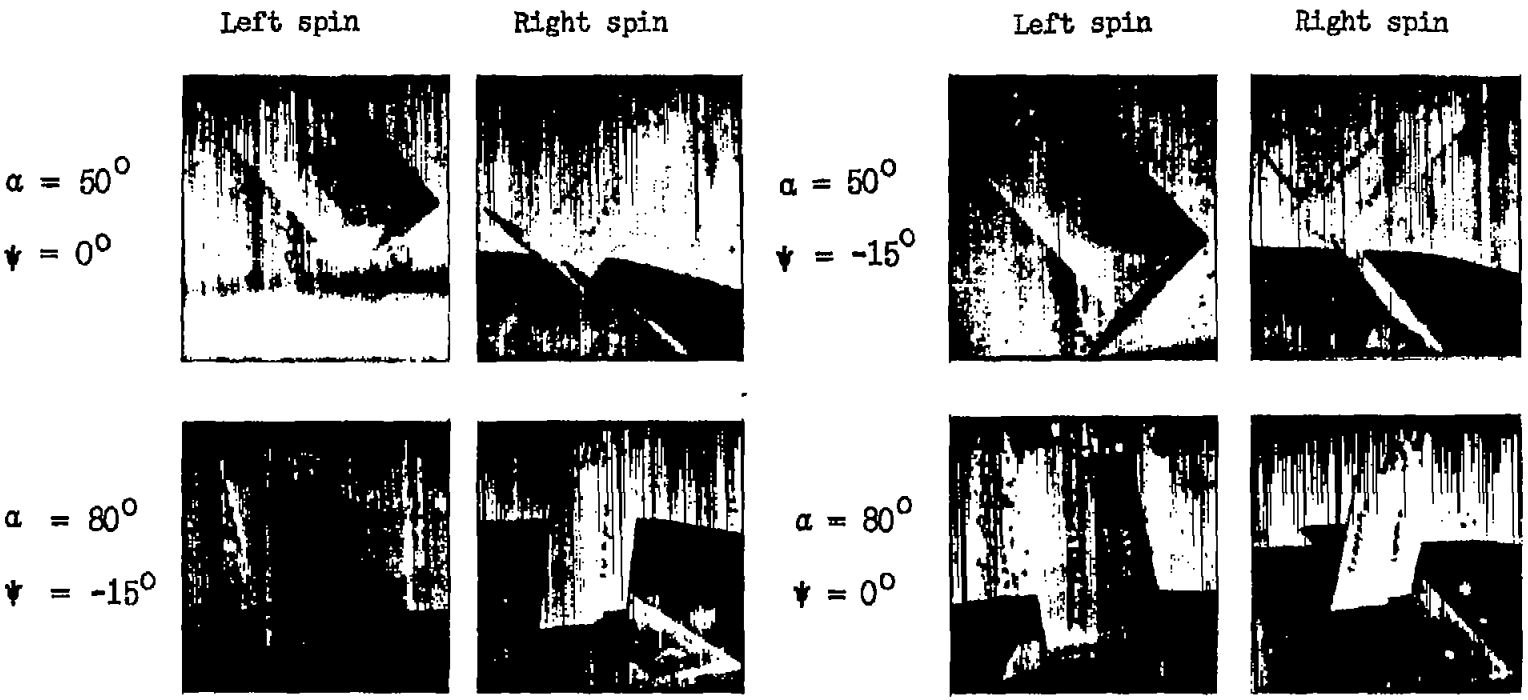

Figure 16.- Concluded.

NATIONAL ADVISORY COMMITTEE FOR AERONAUTICS
LANGLEY MEMORIAL AERONAUTICAL LABORATORY - LANGLEY FIELD, VA

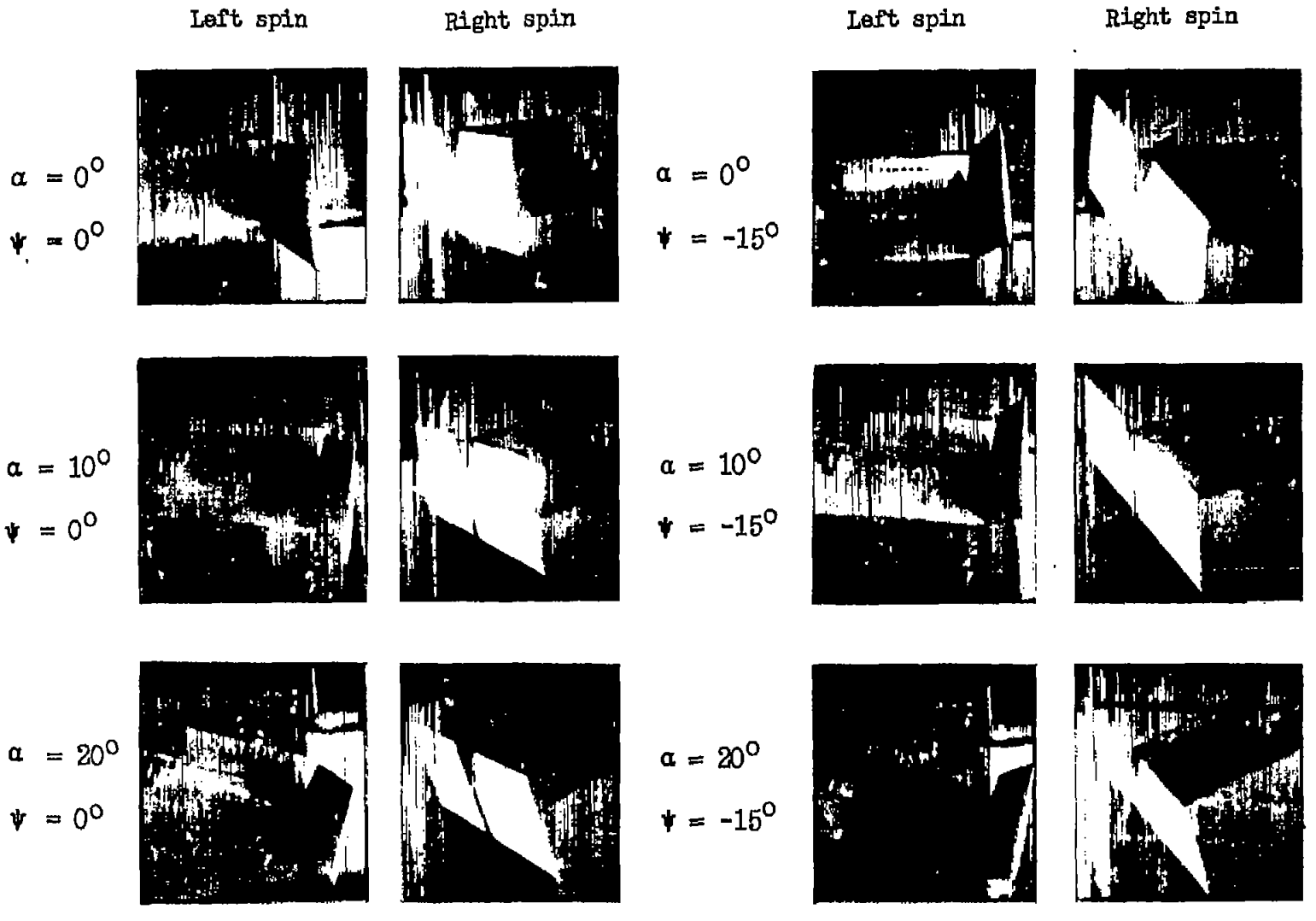

Figure 17.- Photographs of tuft tests performed on vertical tail in combination with horizontal tail in Langley 15-foot free-spinning tunnel. Horizontal tail is in position II.

NATIONAL ADVISORY COMMITTEE FOR AERONAUTICS
LANGLEY MEMORIAL AERONAUTICAL LABORATORY - LANGLEY FIELD, VA

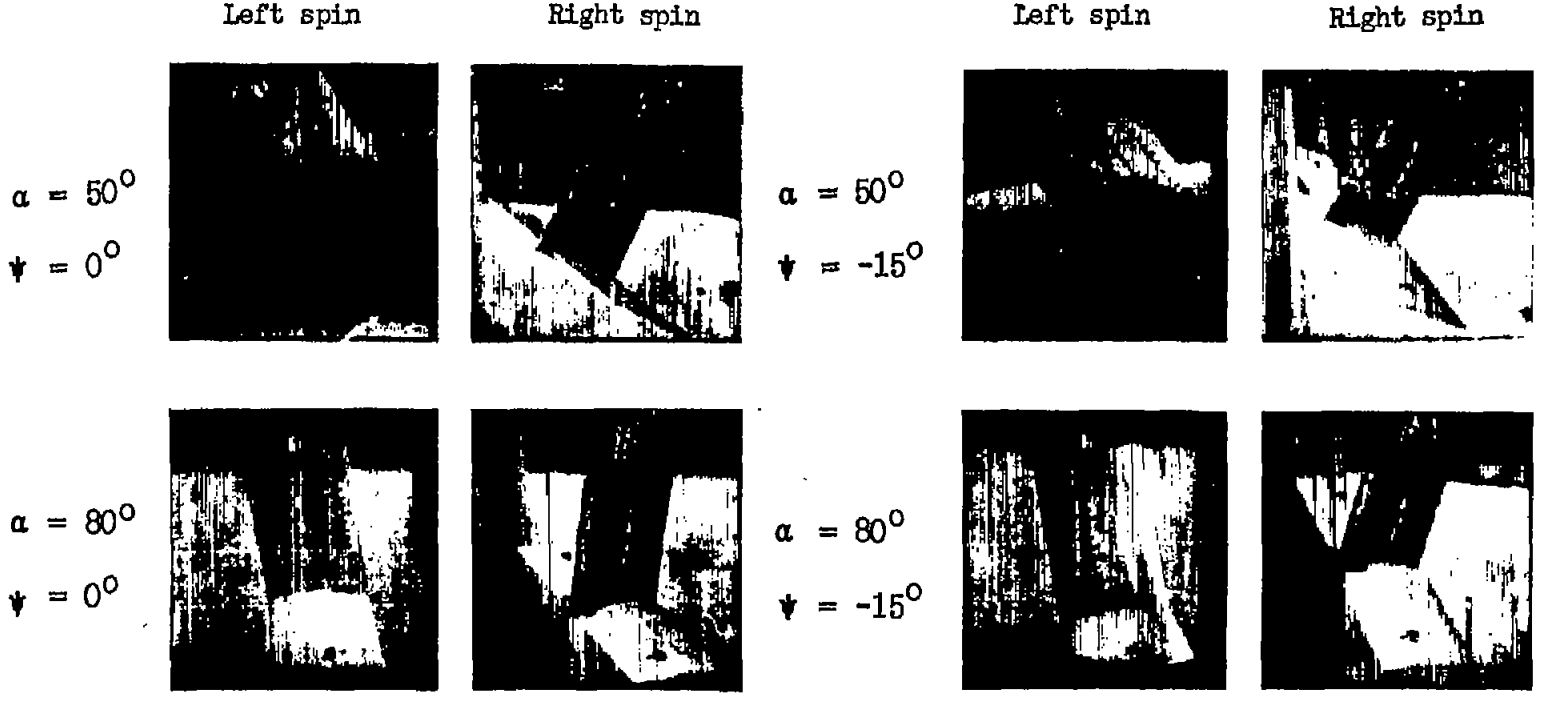

Figure 17.- Concluded.

NATIONAL ADVISORY COMMITTEE FOR AERONAUTICS
LANGLEY MEMORIAL AERONAUTICAL LABORATORY - LANGLEY FIELD VA

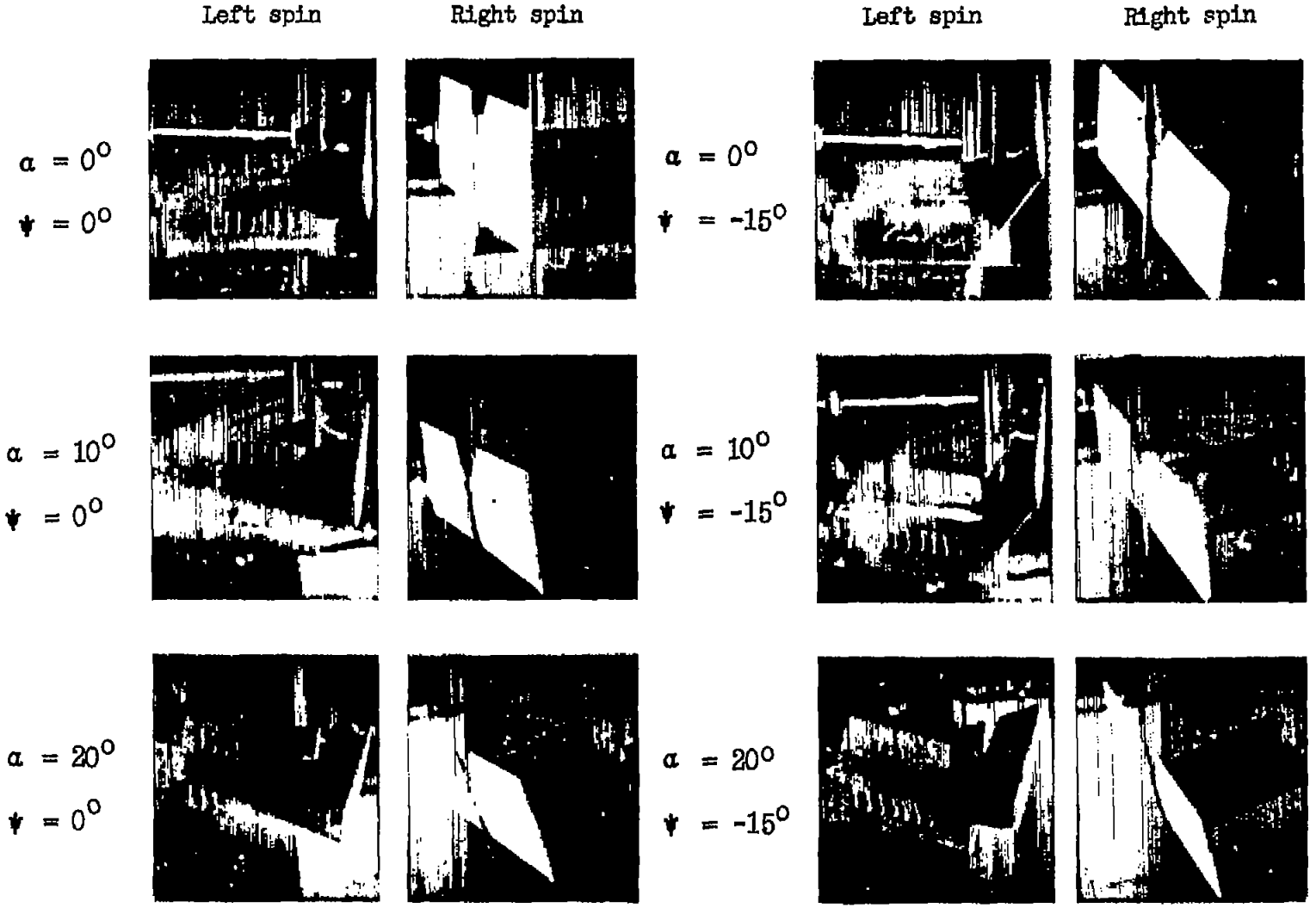

Figure 18.- Photographs of tuft tests performed on vertical tail in combination with horizontal tail in Langley 15-foot free-spinning tunnel. Horizontal tail is in position III.

NATIONAL ADVISORY COMMITTEE FOR AERONAUTICS
LANGLEY MEMORIAL AERONAUTICAL LABORATORY - LANGLEY FIELD, VA.

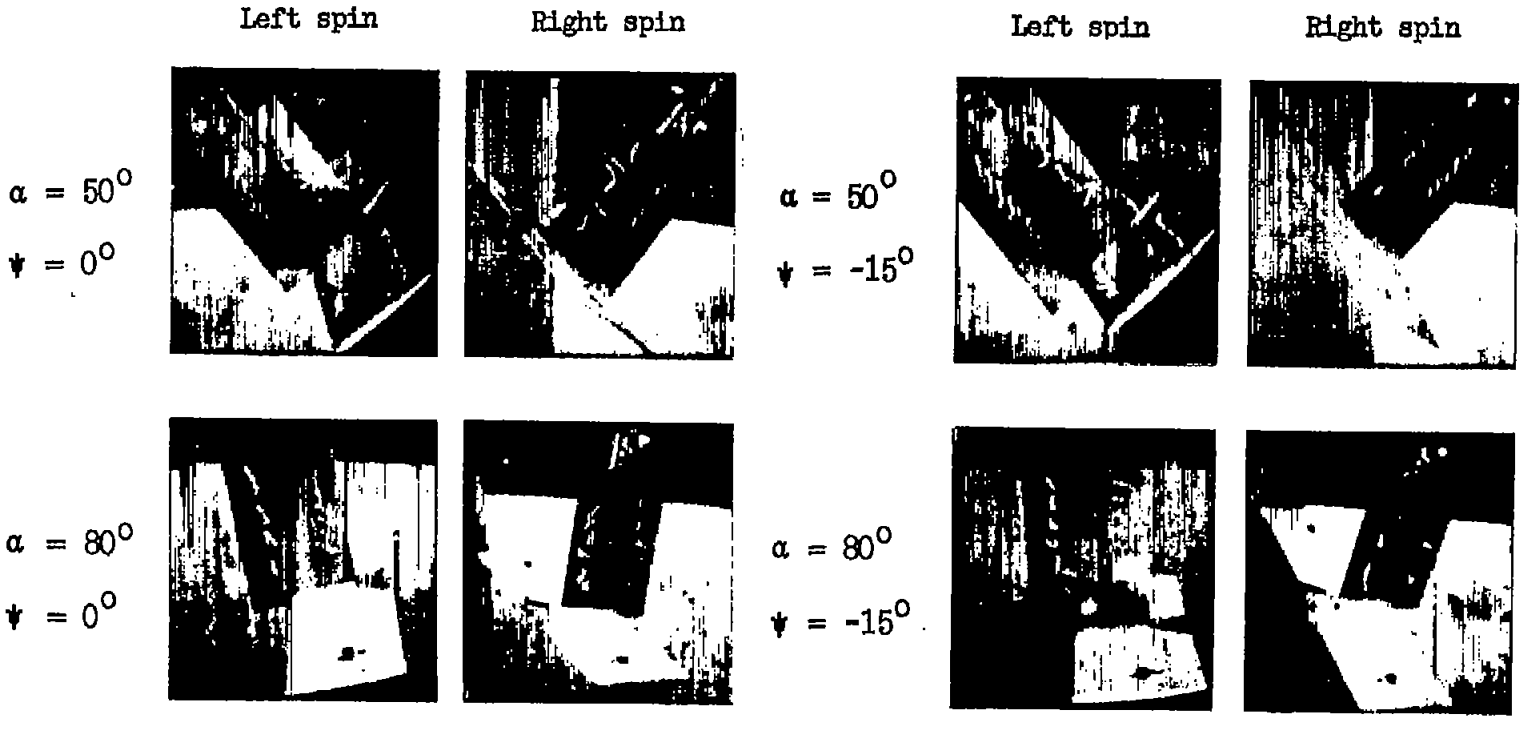

Figure 18.- Concluded.

NATIONAL ADVISORY COMMITTEE FOR AERONAUTICS
LANGLEY MEMORIAL AERONAUTICAL LABORATORY - LANGLEY FIELD VA

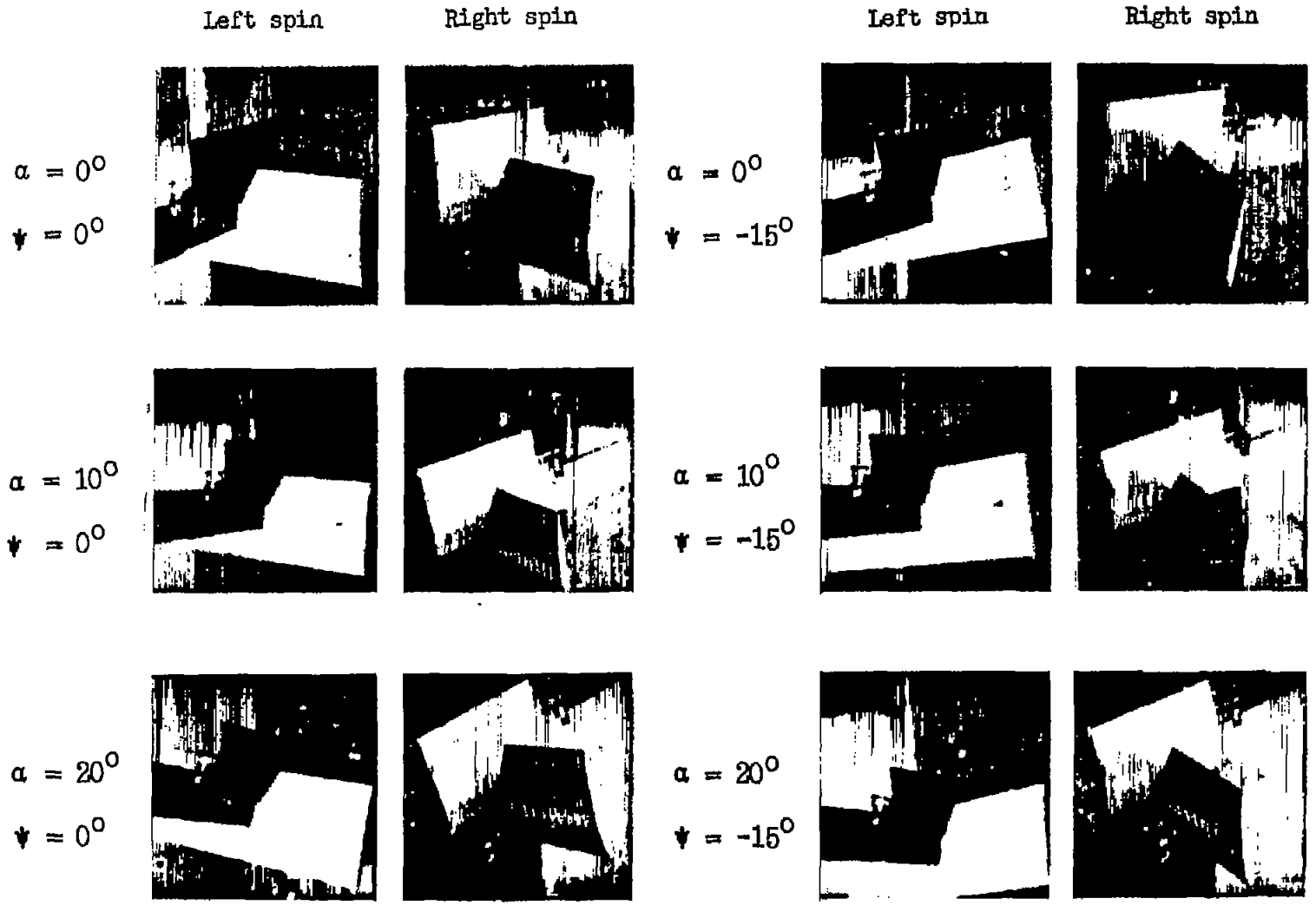

Figure 19.- Photographs of tuft tests performed on vertical tail in combination with horizontal tail in Langley 15-foot free-spinning tunnel. Horizontal tail is in position IV.

NATIONAL ADVISORY COMMITTEE FOR AERONAUTICS
LANGLEY MEMORIAL AERONAUTICAL LABORATORY - LANGLEY FIELD, VA

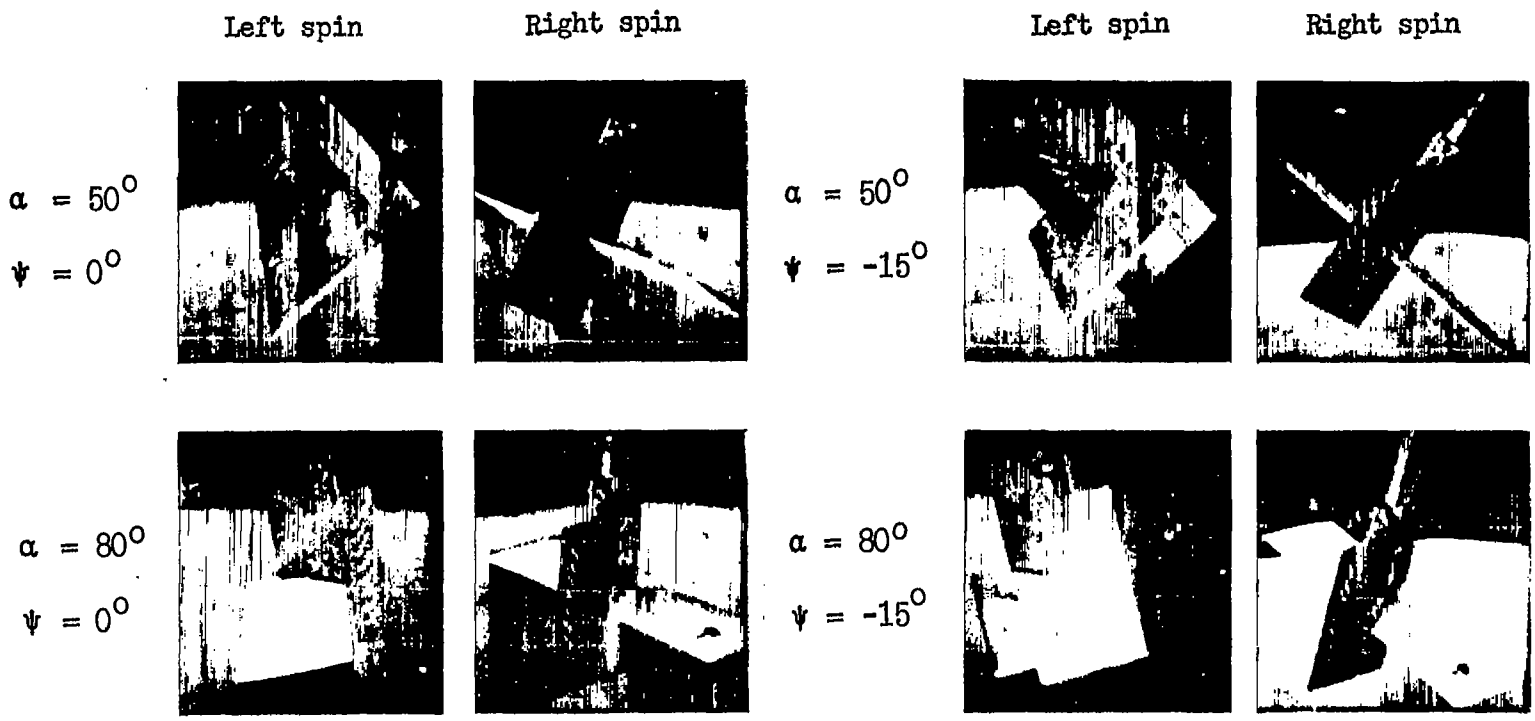

Figure 19.- Concluded.

NATIONAL ADVISORY COMMITTEE FOR AERONAUTICS
LANGLEY MEMORIAL AERONAUTICAL LABORATORY - LANGLEY FIELD VA

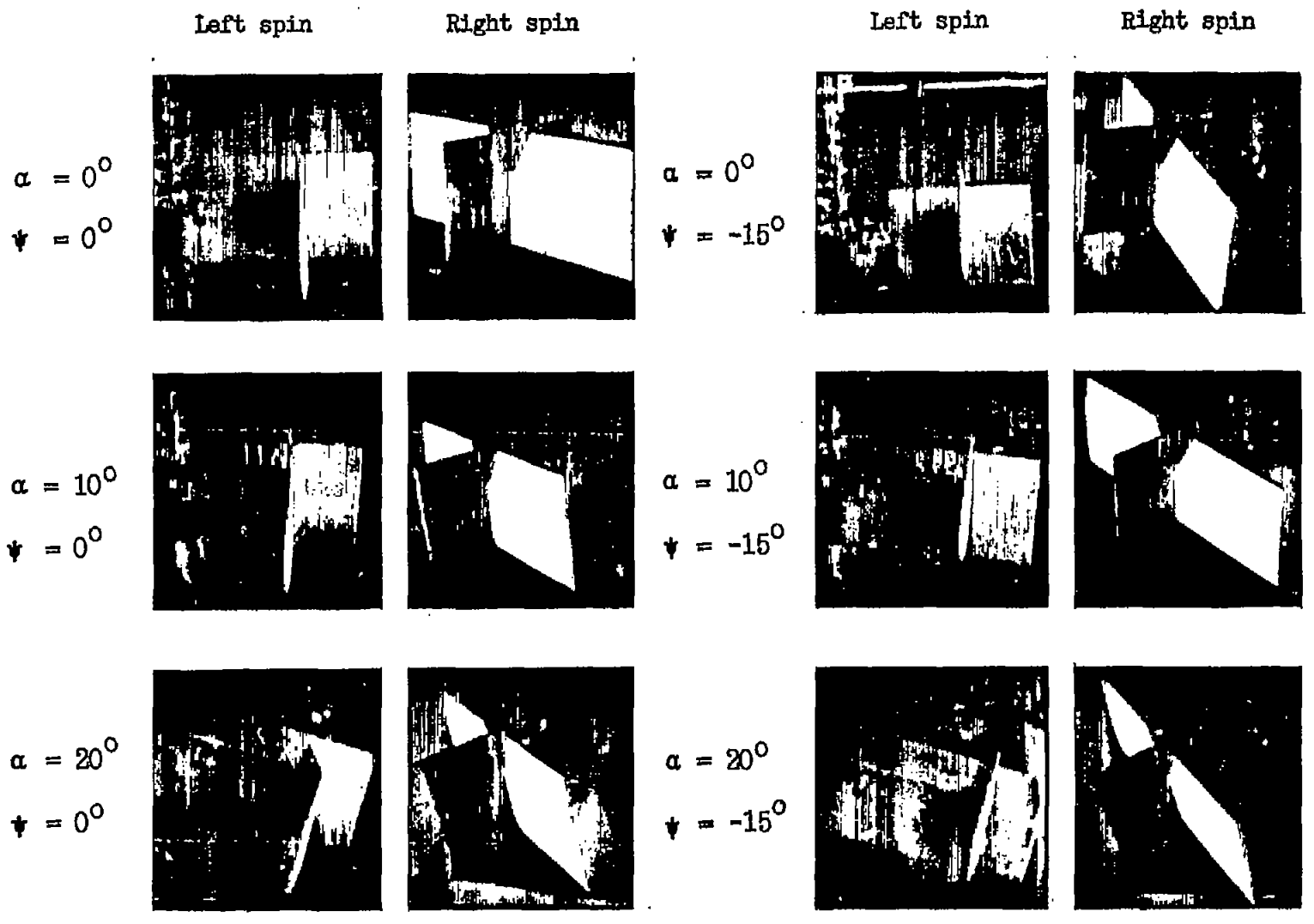

Figure 20.- Photographs of tuft tests performed on vertical tail in combination with horizontal tail in Langley 15-foot free-spinning tunnel. Horizontal tail is in position V.

NATIONAL ADVISORY COMMITTEE FOR AERONAUTICS
LANGLEY MEMORIAL AERONAUTICAL LABORATORY - LANGLEY FIELD, VA

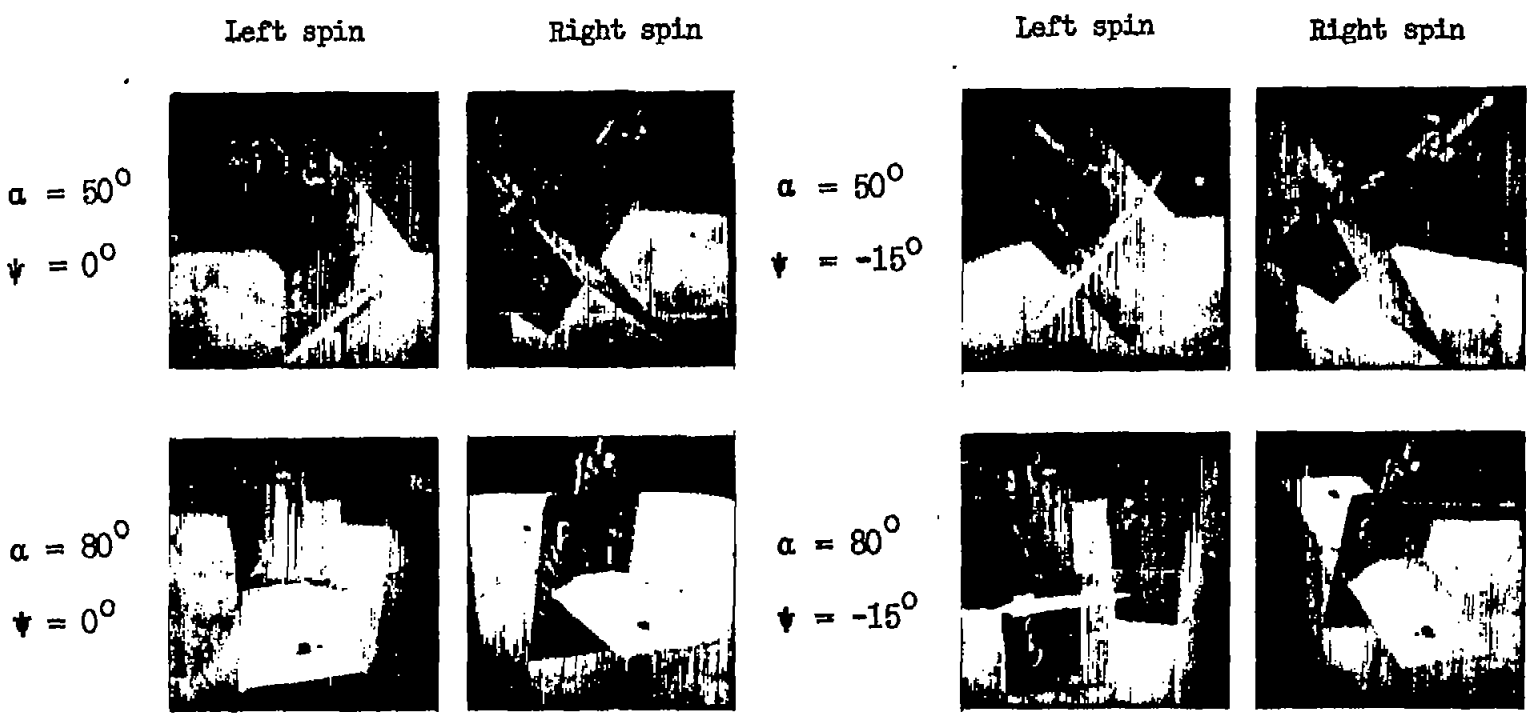

Figure 20.- Concluded.

NATIONAL ADVISORY COMMITTEE FOR AERONAUTICS
LANGLEY MEMORIAL AERONAUTICAL LABORATORY - LANGLEY FIELD, VA.

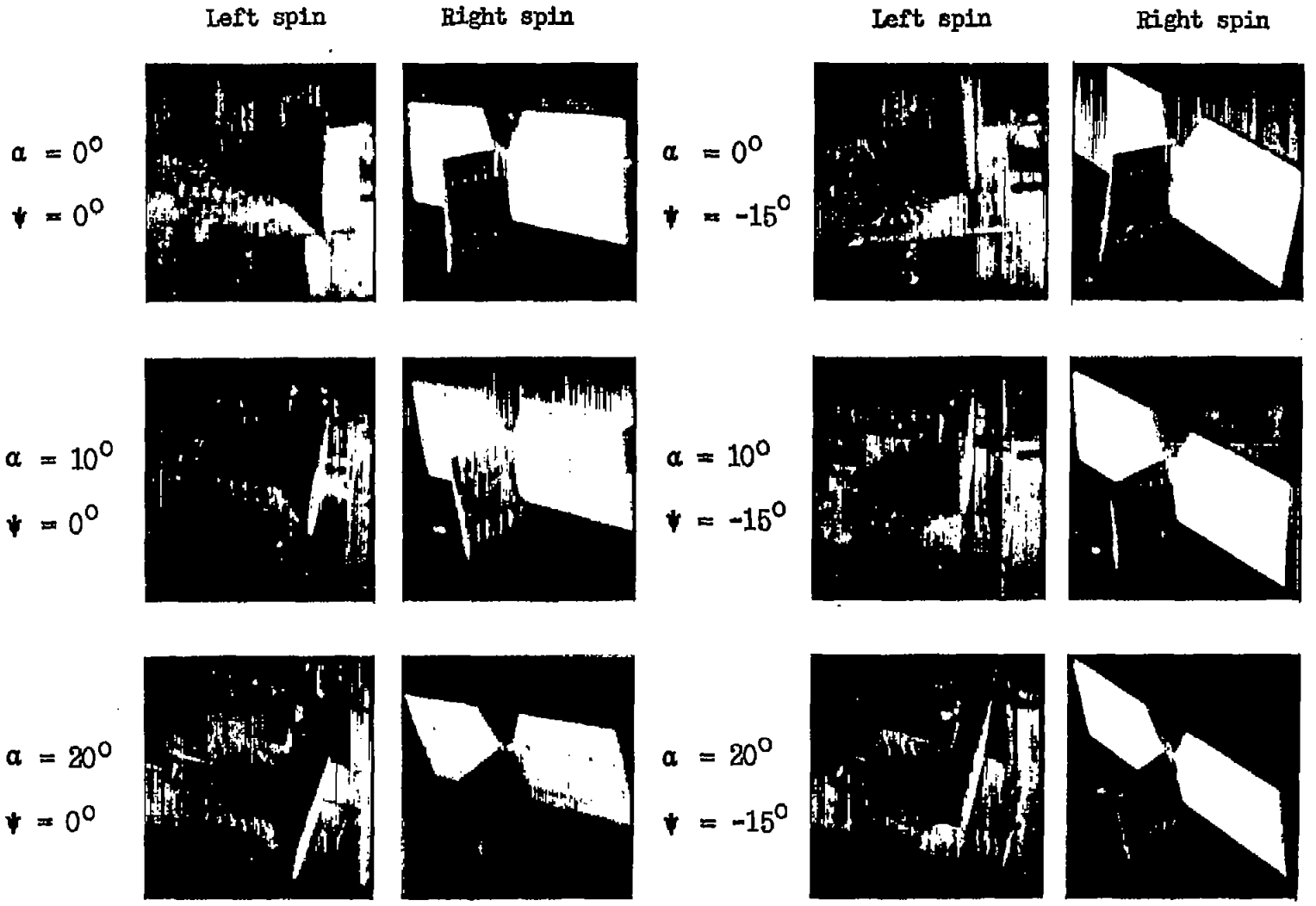

Figure 21.- Photographs of tuft tests performed on vertical tail in combination with horizontal tail in Langley 15-foot free-spinning tunnel. Horizontal tail is in position VI.

NATIONAL ADVISORY COMMITTEE FOR AERONAUTICS
LANGLEY MEMORIAL AERONAUTICAL LABORATORY - LANGLEY FIELD, VA

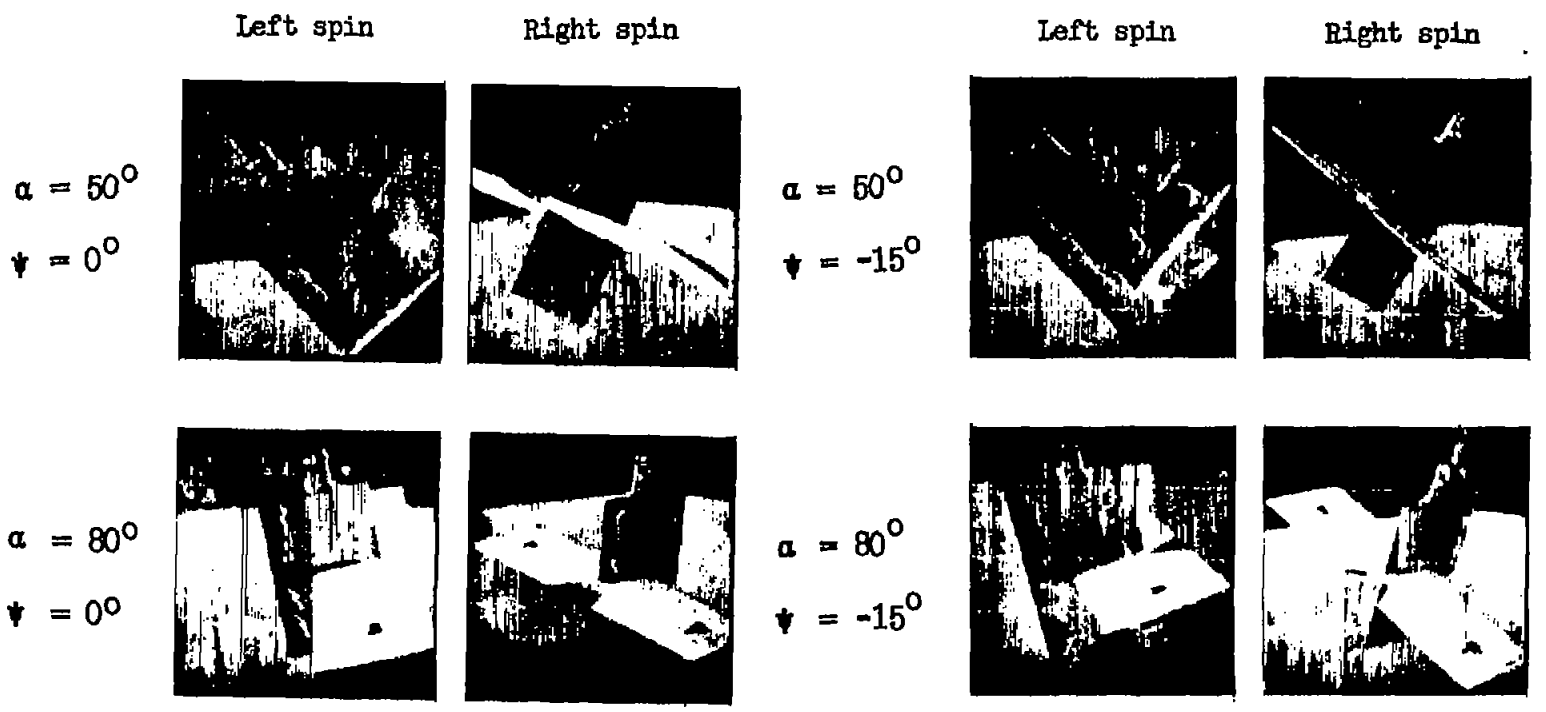

Figure 21.- Concluded.

NATIONAL ADVISORY COMMITTEE FOR AERONAUTICS
LANGLEY MEMORIAL AERONAUTICAL LABORATORY - LANGLEY FIELD, VA

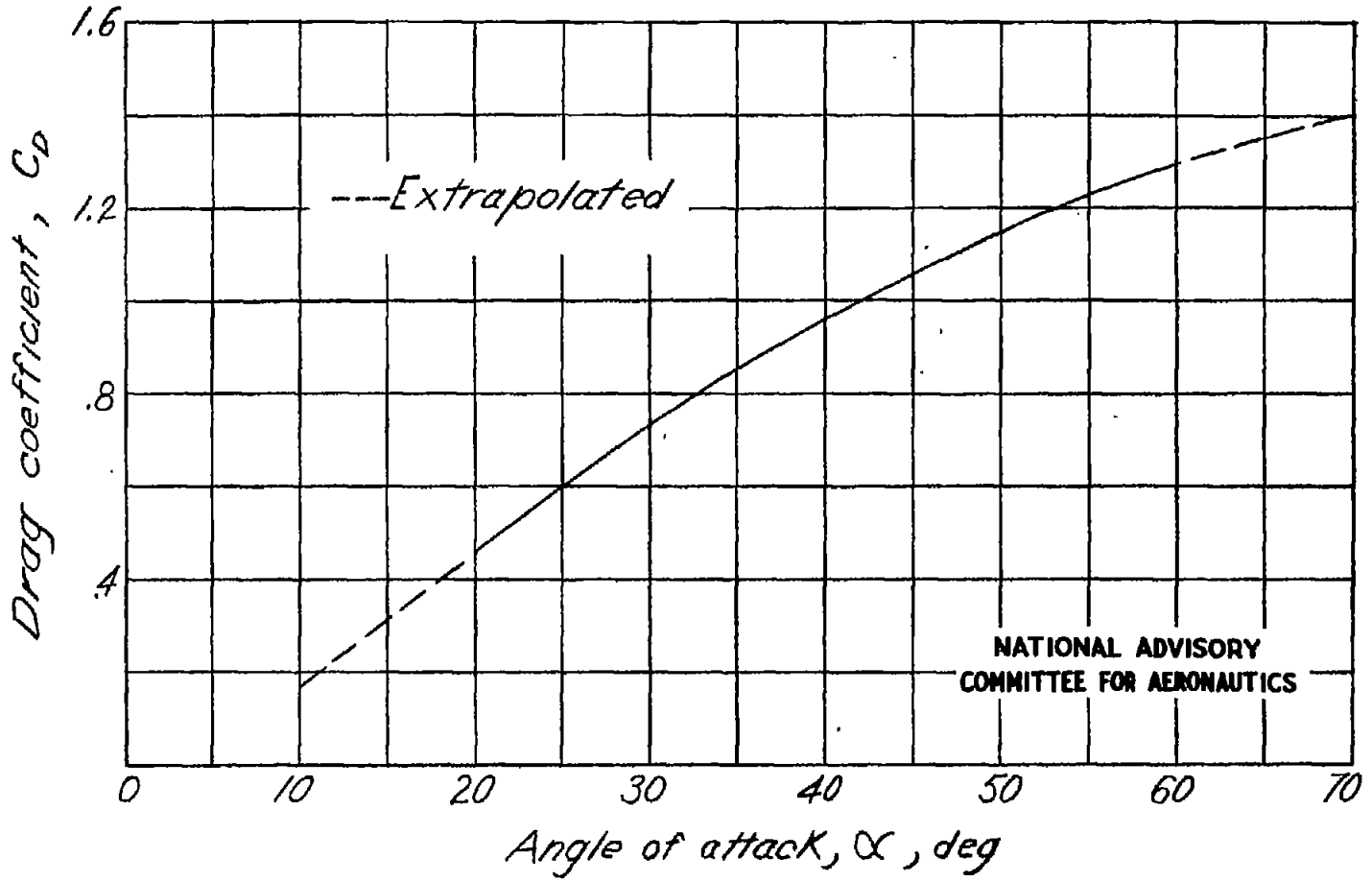

Figure 22.- Variation of drag coefficient with angle of attack for a spinning airplane.

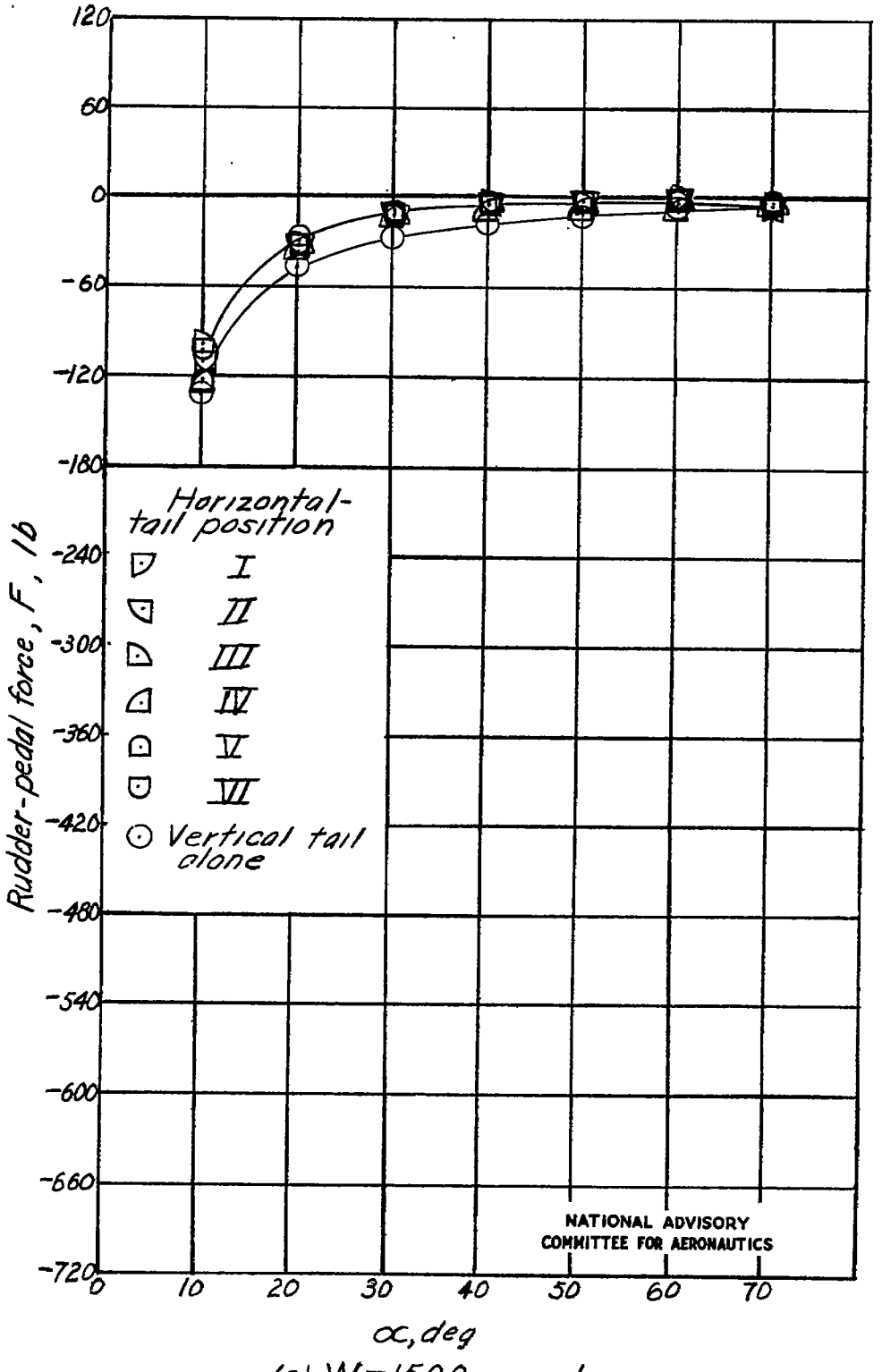

(a) $W = 1500$ pounds.

Figure 23.- Variation of rudder-pedal force with angle of attack for various positions of horizontal tail and for vertical tail alone. ρ, taken arbitrarily at an altitude of 15,000 feet; $\beta = 0^\circ$; $\delta_r = 30^\circ$.

Keyed symbols do not represent test data but are used to distinguish horizontal-tail positions.

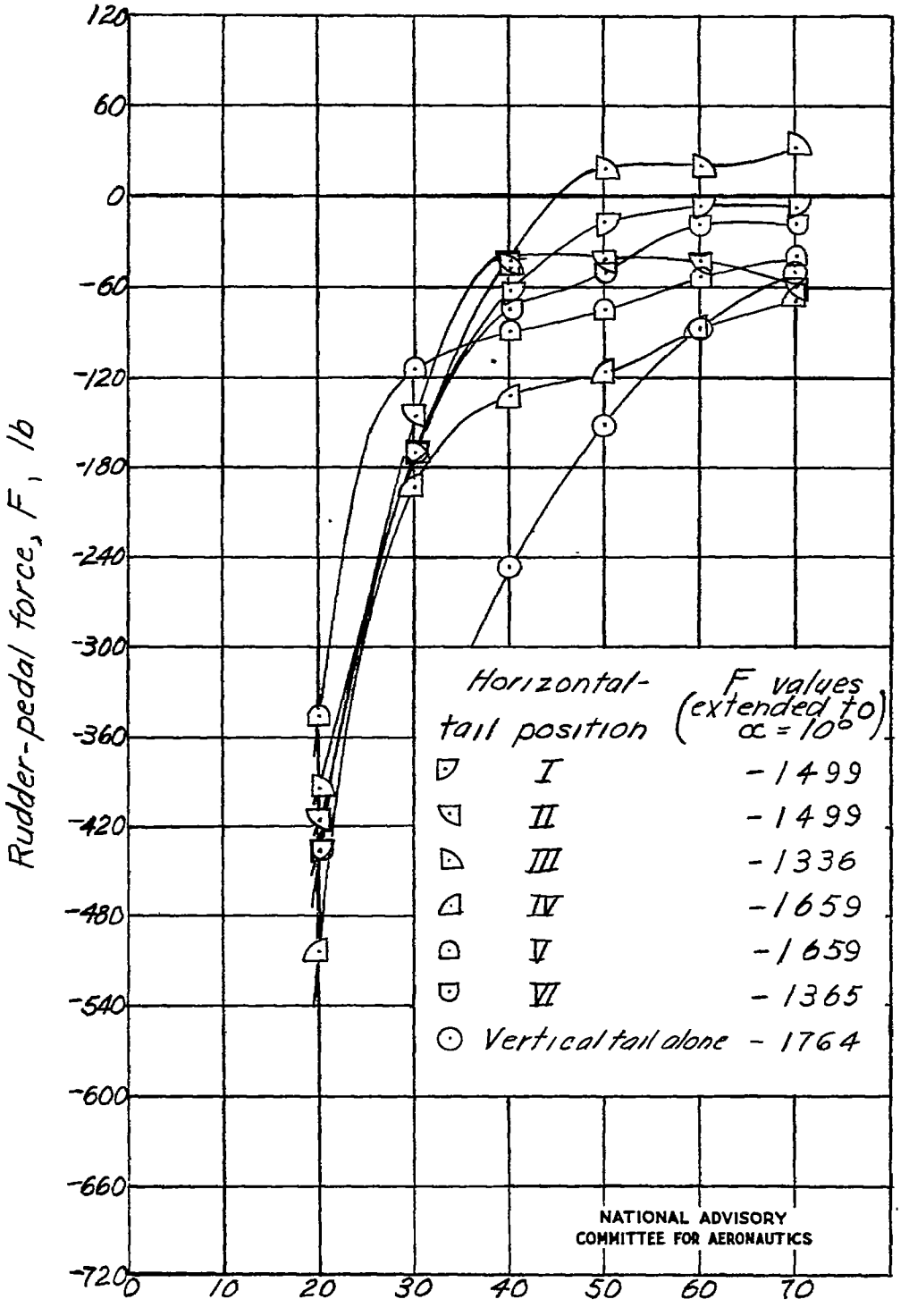

(b) W = 10,000 pounds.

Figure 23.- Continued.

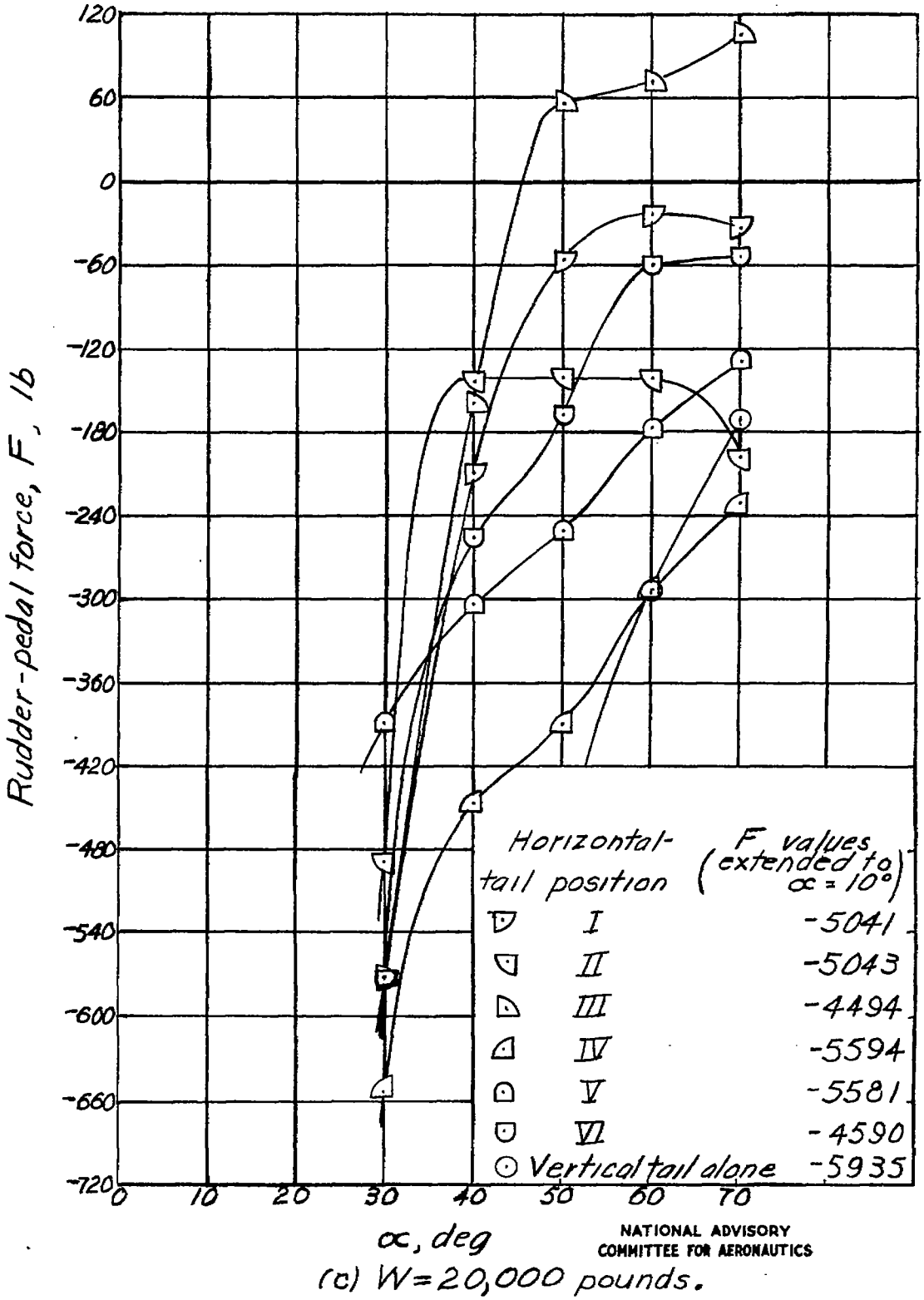

(c) W = 20,000 pounds.

Figure 23.- Concluded.